Title

Projecting 21st century snowpack trends in western USA mountains using variable-resolution CESM

Journal

Climate Dynamics, 50(1-2)

ISSN

0930-7575

Authors

Rhoades, Alan M
Ullrich, Paul A
Zarzycki, Colin M

Publication Date

2018

DOI

10.1007/s00382-017-3606-0

Peer reviewed

Clim Dyn (2018) 50:261–288
DOI 10.1007/s00382-017-3606-0

Projecting 21st century snowpack trends in western USA mountains using variable-resolution CESM

Alan M. Rhoades[1] · **Paul A. Ullrich**[1] · **Colin M. Zarzycki**[2]

Received: 22 August 2016 / Accepted: 26 February 2017 / Published online: 24 March 2017

Abstract Climate change will impact western USA water supplies by shifting precipitation from snow to rain and driving snowmelt earlier in the season. However, changes at the regional-to-mountain scale is still a major topic of interest. This study addresses the impacts of climate change on mountain snowpack by assessing historical and projected variable-resolution (VR) climate simulations in the community earth system model (VR-CESM) forced by prescribed sea-surface temperatures along with widely used regional downscaling techniques, the coupled model intercomparison projects phase 5 bias corrected and statistically downscaled (CMIP5-BCSD) and the North American regional climate change assessment program (NARCCAP). The multi-model RCP8.5 scenario analysis of winter season SWE for western USA mountains indicates by 2040-2065 mean SWE could decrease −19% (NARCCAP) to −38% (VR-CESM), with an ensemble median change of −27%. Contrary to CMIP5-BCSD and NARCCAP, VR-CESM highlights a more pessimistic outcome for western USA mountain snowpack in latter-parts of the 21st century. This is related to temperature changes altering the snow-albedo feedback, snowpack storage, and precipitation phase, but may indicate that VR-CESM resolves more physically consistent elevational effects lacking in statistically downscaled datasets and teleconnections that are not captured in limited area models. Overall, VR-CESM projects by 2075–2100 that average western USA mountain snowfall decreases by −30%, snow cover by −44%, SWE by −69%, and average surface temperature increase of +5.0 °C. This places pressure on western USA states to preemptively invest in climate adaptation measures such as alternative water storage, water use efficiency, and reassess reservoir storage operations.

Keywords Climate change · Western USA · Mountain snowpack · Regional climate modeling · Variable-resolution climate modeling · Elevation-dependent warming

1 Introduction

The 21st century will continue to see unprecedented and irrefutable changes to the climate system (Field et al. 2014). These trends are well understood at the global scale but can be difficult or impossible to use for informing conclusions at regional and/or local scales, in large part because of topographically-driven microclimatic effects. Unfortunately, the majority of presently available climate projections using global climate models (GCMs) are constrained to resolutions of 1° for multi-decadal and large ensemble modeling endeavors (Taylor et al. 2012; Kay et al. 2015). In

This research was funded by the National Science Foundation (NSF) via the Climate Change, Water, and Society Integrated Graduate Education and Research Traineeship (IGERT) program at the University of California, Davis (NSF Award Number: 1069333), the Leland Roy Saxon and Georgia Wood Saxon Fellowship, the "Multiscale Methods for Accurate, Efficient, and Scale-aware Models of the Earth System" within the Director, Office of Science, Office of Biological and Environmental Research of the US Department of Energy Earth System Modeling Program (ESM) under Contract No. DE-AC02-05CH11231. Support also comes from the California Agricultural Experiment Station (project CA-D-LAW-2203-H).

✉ Alan M. Rhoades
amrhoades@ucdavis.edu

[1] Department of Land, Air, and Water Resources (LAWR), University of California, Davis, Davis, CA, USA

[2] National Center for Atmospheric Research, Boulder, CO, USA

recent years there has been a push towards finer resolutions, and some long-term simulations have achieved resolutions of 0.5–0.25°; however, for many of these studies the output fields and focus are limited to a specific scientific inquiry (Wehner et al. 2010; Kinter et al. 2013; Bacmeister et al. 2014; Small et al. 2014b; Harris et al. 2016). This resolution barrier has largely been due to constraints in computing power, simulation throughput and data storage. Thus, climate projections necessary for management and planning at the regional level are still needed.

The unmet need for local-scale data poses additional risks within the western USA where regional climate change is directly altering snowpack totals. Snowpack is intrinsic to western USA hydrology representing three-fourths of the freshwater supply (Palmer 1988; Cayan 1996). Under global climate change projections over the coming century, temperatures will continue to rise, snowpack totals will decline, higher precipitation-to-snowfall ratios will occur, peak snowpack accumulation will occur earlier in the season, record-setting low snowpack totals will continue to be set, and natural freshwater storage [i.e., snow water equivalent (SWE)] will continue to diminish (Mote et al. 2005; Bales et al. 2006; Barnett et al. 2008; Pavelsky et al. 2011; Kapnick and Hall 2012; Pavelsky et al. 2012; Salzmann and Mearns 2012; Wise 2012; Ashfaq et al. 2013; Diffenbaugh et al. 2013; Pierce and Cayan 2013; Rupp et al. 2013; Berghuijs et al. 2014; Klos et al. 2014; Berg et al. 2015; Lute et al. 2015; Belmecheri et al. 2016). This will impact both the timing and magnitude of summer streamflows, which are essential in meeting agricultural water demand, providing a steady energy supply, and sustaining ecosystem function. For example, the 2014–2015 snow season was the driest year on record in California (5% of normal) over a 500 year period (Belmecheri et al. 2016), with water reserves at record lows and repercussions felt throughout California, especially in low-income agricultural communities in the Central Valley such as the Tulare Basin. Snowpack decline is especially important in the western USA energy sector where renewables (e.g., hydroelectric power) provide 56% of generating capacity and energy development plans haven't included future climate impacts, potentially disrupting the ability of energy providers to consistently meet future electricity demand (Bartos and Chester 2015). If anthropogenic emissions continue unabated, the drivers of hydroclimatic change could accelerate (Ashfaq et al. 2013), resulting in an increased number of low-to-no snow total years (Diffenbaugh et al. 2013) by the late 21st century.

Climate change will directly impact mountain snowpack in three ways. First, warmer temperatures will lead to an earlier spring thaw, increasing spring season runoff from snowmelt and decreasing late summer water availability. Second, in accordance with the Clausius–Clapeyron relationship, warmer air holds more water and so leads to potential increases in large-scale precipitation in areas with forced orographic uplift and warmer temperatures also tend to favor rainfall over snowfall. This is of particular importance to the western USA where 20–40% of precipitation events occur at or around freezing (−3 to 0 °C) (Bales et al. 2006), making snowfall particularly susceptible to end-of-century projections of warming between +1.4 and 5.4 °C (National Climate Assessment 2016). Along the leeward (eastern) portion of the Sierra Nevada, an increase of 6 °C would threaten the majority of Sierra Nevada snowpack (above 3000 m) and a 2 °C increase could shorten the snow season by a full month (Bales et al. 2014). Rising surface temperatures are particularly important in the spring months at mid- to high-elevations, which would normally be below freezing throughout the winter period (Cayan 1996; Stewart 2009). These changes are further enhanced by the snow-albedo feedback, which plays a pivotal role in determining the local and global radiative balances (Anderson 1976; Hall 2004; Qu and Hall 2014). The global radiative forcing associated with this feedback, shown in recent GCM simulations for the IPCC (CMIP5), was found to be between 0.03 and 0.16 W/m^2/K (Qu and Hall 2014). Although not as substantive as the cloud-albedo (−0.55 W/m^2) and aerosol (−0.27 W/m^2) feedbacks, the snow-albedo feedback is nonetheless important, especially in the northern latitudes (Field et al. 2014).

Regional climate models (RCMs) have been an instrumental stopgap in addressing the discrepancy between coarse-resolution global simulations and the need for local-scale climate information. However, these models have their own limitations (and associated uncertainties) derived from the necessity of using a GCM forcing dataset (bias propagation), lateral boundary relaxation strategies (introducing artificial noise), and lack the global-to-regional dynamic coupling that may be required to understand multi-decadal climate change feedbacks, such as atmosphere-ocean teleconnections. Methods such as bias correction have been employed to alleviate some of the uncertainty associated with coupling global datasets with regional models (Ashfaq et al. 2013; Pierce and Cayan 2013), but these corrective techniques are often only applicable in a limited context and are difficult to apply to future projections without assuming stationarity [i.e., that historical trends can describe future trends; Velázquez et al. (2015)], or adding compensating biases (Cannon et al. 2015; Pierce et al. 2015). Statistical downscaling has also been useful for generating climate data at high resolutions, and has been invaluable to management and planning organizations due to its low computational cost (Groves et al. 2008; Maurer et al. 2010; Pierce et al. 2013; Chen et al. 2014b; Berg et al. 2015). However, statistical downscaling typically relies on stationarity assumptions which

may not hold under a changing climate. Further, it has been shown that using relatively coarse GCM data can lead to incorrect statistical inference and biased regional information, especially for precipitation (Chen et al. 2014b; Berg et al. 2015) due to differences in seasonality and phenomenon causing extreme precipitation at different GCM resolutions (van der Wiel et al. 2016). Thus, the development of accurate regional climate change projections remains a major scientific problem and the associated uncertainties associated have yet to be fully constrained, especially in the hydrologic sector (Groves et al. 2008).

To advance the scientific understanding on this topic, and further constrain the magnitude, extent, and spatial distribution of snowpack change, the authors have utilized a global-to-regional downscaling technique known as variable-resolution (VR) within the community earth system model (VR-CESM). This technique utilizes a global coarse resolution grid which is then horizontally refined over a specific area of interest; hence, VR-CESM often requires 10% of the computing power of a conventional uniform resolution global model simulated at high resolution. VR capabilities have now been incorporated in operational GCMs across many major modeling centers (Skamarock et al. 2012; Harris and Lin 2013; Zarzycki et al. 2014b; McCorquodale et al. 2015). To date, VR has been proven effective for assessing regional climate (Rauscher et al. 2013; Huang et al. 2016; Rhoades et al. 2016; Huang and Ullrich 2016), large-scale weather systems (Rauscher and Ringler 2014), and tropical cyclones (Zarzycki and Jablonowski 2014; Zarzycki et al. 2014a, 2015). The multi-scale approach of VR-CESM allows it to serve as a bridge between GCMs and RCMs and overcome many of the known issues with conventional downscaling methods. Namely, VR has the ability to provide high-resolution in a desired area, eliminates multi-model lateral boundary forcings (and propagated bias) used in conventional global-to-regional modeling pursuits, captures global teleconnections, and has a higher simulation throughput and smaller data storage demand when compared to standard uniform-resolution GCMs. Added benefits of VR-CESM are also discussed in greater detail in Rhoades et al. (2016), where multi-year climate integrations were performed using a small university server (<1000 cores), with 20–40 day turnarounds on 25 year simulation periods at resolutions of 0.25° (28 km) to 0.125° (14 km). The VR grid used for this study focuses on the western USA and is shown in Fig. 1, telescoping from a globally quasi-uniform 1° resolution to a refined 0.25° region. Like other downscaling strategies, VR-CESM sub-grid-scale physics are still being vetted down to extremely high-resolutions (i.e., <28 km) to assess scale sensitivity (Zarzycki et al. 2014b) and, currently, VR-CESM is not supported to be run at non-hydrostatic (<10 km) scales. Therefore, if VR-CESM data is to be used for assessment and planning at local scales it may be advantageous to use a bias-correction technique prior to using the VR-CESM data in any impact study.

The structure of the remainder of the paper is as follows: Sect. 2 contains information about the experimental design including specifications about VR-CESM, the VR-CESM forcing datasets, and the ensemble of datasets used to intercompare the magnitude, extent, and spatial distribution of change facing western USA snowpack totals in relation to VR-CESM. Section 3 highlights the pre-2005 climate daily average comparisons between the various datasets to identify potential bias originating from structural uncertainties. Section 4 presents the graphical and statistical intercomparion of SWE between the global-to-regional datasets. Section 5 provides a more comprehensive analysis of VR-CESM snowpack trends at both seasonal and multidecadal time frames. Lastly, Sect. 6 discusses conclusions and future work.

2 Experimental design

2.1 CESM specifications

The community earth system model (CESM), version 1.2.2, was utilized for this research. CESM is a widely-used and community-supported climate model developed at the National Center for Atmospheric Research (NCAR) and the US Department of Energy (DoE). Representations of each of the major Earth system components, including the atmosphere, land surface, land-ice, ocean, ocean-wave, river run-off and sea-ice, are available in CESM. This study used the F-component set, FAMIPC5, which is standard practice for the atmospheric model intercomparison project (AMIP) (Gates 1992). The F-component set couples the prognostic atmosphere (community atmosphere model version 5.3, CAM5) (Neale et al. 2010) and land-surface (community land model version 4.0 with satellite phenology, CLM4-SP) (Oleson et al. 2010) while using prescribed sea-surface temperatures (SSTs) and sea-ice extent in place of dynamic ice and ocean models. The use of prescribed SSTs allows for more accurate surface forcing when compared to simulations with dynamic ocean and sea-ice and reduces computational and data storage space requirements.

Within CAM5, the spectral element (CAM5-SE) dynamical core was used for this work (Taylor et al. 1997; Dennis et al. 2011). CAM5-SE is built with a continuous Galerkin spectral finite-element method to solve the hydrostatic atmospheric primitive equations. CAM5-SE has several demonstrable benefits compared with the other CAM dynamical cores, including unstructured grid support that eliminates grid singularities at higher latitudes, and near-perfect multi-processor scalability (Taylor and Fournier

2010; Dennis et al. 2011; Zarzycki et al. 2014a, b; Zarzycki and Jablonowski 2014). Physical parameterizations in CAM5, which simulate forcing due to sub-grid scale processes, include aerosols (Ghan et al. 2012), deep convection (Neale et al. 2008), macrophysics (Park et al. 2014), microphysics (Morrison and Gettelman 2008), radiation (Iacono et al. 2008), and shallow convection (Park and Bretherton 2009). Further details regarding CAM5-SE can be found in Neale et al. (2010).

CLM4-SP uses a subdivision scheme to represent the heterogeneous distribution of glaciers, lakes, urban landscapes, vegetation, and wetlands (Oleson et al. 2010; Lawrence et al. 2011). To accurately describe each grid cell's unique land surface distribution, the moderate resolution imaging spectroradiometer (MODIS) satellite data at 0.5° resolution is used for vegetation and high-resolution surface datasets for soil types, urban expanse, and water bodies. The satellite-derived values for vegetation are aggregated into 16 unique plant functional types (PFTs), including non-vegetated. A detailed PFT representation within each land-unit is critical in capturing snowpack trends, as interactions between the canopy and snowpack are PFT specific for biogeochemical, radiative, and hydrological processes such as interception, throughfall, canopy drip, water removal via transpiration, and optical property interactions based on leaf angle (Lawrence et al. 2011).

The CLM4-SP snowpack model is based on several well established methods including Anderson (1976), Jordan (1991), and Yongjiu and Qingcun (1997). The snowpack model is regarded as one of the more complex (Cai et al. 2014) and is among the best at representing key snowpack variables, such as SWE (Chen et al. 2014a), in the suite of available coupled land-surface models. This is due, in large part, to the discretization of five distinct snow layers that dynamically compact and exchange energy and water. The five-layer model simulates the total life cycle of snowpack including aging and compaction, black carbon and mineral deposition, ice mass, layer thickness, optical properties, temperature profiles, and, importantly for water resources, water mass. As shown, CLM4-SP accounts for many of the key drivers and processes that influence the snowpack life-cycle, however the CLM4-SP snowpack module does have limitations in its ability to represent peak snowpack timing (too early) and melt rate (too fast), especially when compared to point-location in-situ observations (Chen et al. 2014a; Toure et al. 2016; Rhoades et al. 2016).

2.2 VR-CESM forcing datasets

For the VR-CESM simulations, historically prescribed SST and sea-ice fractions were derived from the Hadley Centre sea ice and SST dataset version 1 (HadISST1) and version 2 of the National Oceanic and Atmospheric Administration (NOAA) weekly optimum interpolation (OI) SST analysis (Hurrell et al. 2008) and the future SSTs and sea-ice forcings were derived from a future 1° RCP8.5 bias-corrected dataset (Small et al. 2014a), both of which were developed at NCAR. The bias-correction compares simulated and observed SSTs and assumes that model errors from the historical simulation will be similarly present in future simulations (i.e., quantile mapping). After the bias-correction is applied, the SST and sea-ice fractions were then assessed and quality controlled to ensure consistency between temperature and fractional area coverage were satisfied. Careful consideration of how to best represent future SSTs and sea-ice are crucial as they influence ocean-forced teleconnections that are simulated by the global dynamic atmosphere-land framework of VR-CESM. Teleconnections are key drivers of regional scale variability in western USA wintertime precipitation and snowpack trends (Wallace and Gutzler 1981; Glantz et al. 1991; Dettinger and Cayan 1995; Cayan 1996; Cayan et al. 1999; Pandey et al. 1999). Importantly, several studies have shown that CESM has skill in representing the El Niño Southern Oscillation (ENSO) (DeFlorio et al. 2013; Wang et al. 2014), the Pacific Decadal Oscillation (PDO) (DeFlorio et al. 2013), and the Pacific-North American (PNA) pattern (Li and Forest 2014), all important for the western USA. These teleconnection representations are expected to carry over into VR-CESM.

2.3 VR-CESM model grid and topographical fields

The VR grid was generated using SQuadGen (Ullrich 2014), which uses paving to apply localized refinement to a basic equiangular cubed-sphere followed by spring dynamics for smoothing. An identical grid is used for both CAM and CLM in this research (Fig. 1). To generate the topography for the VR-CESM28 simulation, the ETOPO2v2 (2 km resolution) satellite derived dataset was employed (National Geophysical Data Center 2006). Due to the high-order properties of the dynamical core, smoothing is required to avoid spurious high-frequency noise from the sampled topography. Thus, the original ETOPO2v2 dataset resolution (2 km) was regridded and smoothed slightly beyond the native VR grid resolution (28 km) for numeric stability. This particular issue was discussed in Zarzycki et al. (2015) where excessive terrain roughness in CAM5-SE was shown to produce spurious vertical velocities and numerical artifacts. Therefore, to alleviate this artificial noise the c parameter from Eq. (1) in Zarzycki et al. (2015) was used to smooth the ETOPO2v2 topographic dataset along with repeated applications of fourth-order hyperviscosity. This process produces a topographic representation of the western USA with more smoothing applied in regions

of coarser grid resolution. The resulting topography is a vast improvement over the excessively smoothed topography typically employed by 1° uniform-resolution GCMs (Fig. 2).

2.4 Statistical methods

A key objective of this assessment is to understand the snowpack trends produced by VR-CESM28 from 2025 to 2100 and compare them to widely-used GCM and RCM ensembles. A tabulation of the established climate change datasets used for this intercomparison can be found in Table 1. To standardize the various datasets, climate data operators (CDO), NetCDF operators (NCO), and the NCAR command language (NCL) were used (Schulzweida et al. 2007; Zender 2008). The climate and seasonal averages were computed using a mask of the Cascades, Klamath, Rockies, Sierra Nevada, and Wasatch and Uinta (see Fig. 3). These masks were derived from the EPA's Ecoregions classification system (Ecoregion Level III).

The datasets were further remapped to similar map projections and to the highest resolution needed for proper intercomparison (i.e., 4 km for pre-2005 PRISM comparisons and 14 km for NLDAS/BCSD-CMIP5 RCP8.5 climate change comparisons). Remapping from coarser to finer horizontal resolution was chosen to allow for equal comparisons between western USA mountain shapefile masks without degrading high-resolution spatial information and to ensure that proper statistical sampling of 250–500 m elevational band trends could be made. To do this, the earth system modeling framework (ESMF) capabilities in the NCAR command language (NCL) and TempestRemap (Ullrich and Taylor 2015; Ullrich et al. 2016) software suites were used. Summary statistics for the five mountain ranges were calculated for each of the datasets, including mean, standard deviation, lower quartile, median, upper quartile, and maximum. The Wilcoxon–Mann–Whitney rank-sum test was applied to assess statistical significance of differences between time periods.

2.5 Climate change datasets used for western USA intercomparison

To robustly assess the range of potential outcomes that the RCP8.5 scenario may have on western USA mountain snowpack an intercomparison of the various modeling methodologies (e.g., dynamical, statistical and traditional GCM) was conducted. The datasets were chosen based on public availability and use in the literature. Brief descriptions of the various climate datasets are outlined below.

VR-CESM28 was executed on the local UC Davis Climate Cluster from 1980 to 2005 and 2025 to 2100, under the IPCC RCP8.5 scenario. Daily average outputs were created for select variables in CAM and CLM, including those featured in the analysis of this paper. Additional climatological simulations have been produced by varying the initial conditions, but are not included in this analysis (Rhoades et al. 2016; Huang et al. 2016; Huang and Ullrich 2016). Importantly, in the VR-CESM analyses mentioned it was found that it takes approximately 20–30 DJF simulated months (7–10 simulated years) for the median California precipitation trends to converge around a median value (across a multitude of VR-CESM resolutions). Thus, it is inferred that these trends will hold throughout all western USA mountain ranges and the 26 year historical baseline simulation is sufficient to ensure that natural variability (e.g., ENSO and PDO) is taken into account.

The Coupled Model Intercomparison Project, Phase 5, (CMIP5) incorporates over 20 modeling centers worldwide. For the model intercomparison, the eight CESM family ensemble members were utilized to create an ensemble average. The ensemble consists of six community climate system model (CCSM) 4.0 members (an earlier version of CESM), one CESM1 Biogeochemistry (BGC) member (the full carbon cycle version of CESM), and one CESM1 CAM5 member (the latest production version of CESM).

The North American Regional Climate Change Assessment Program (NARCCAP) is an RCM ensemble

Table 1 Western USA climate datasets

Climate dataset	Snowpack variable	Spatial resolution (km)	Temporal resolution	Assessed timeframes
VR-CESM28	PRECT, SNOWFALL, SNOWC, SWE, 2 mST	28	Daily	1980–2005, 2025–2100
NLDAS	SWE	14	Daily	1980–2005
PRISM	PRECT, 2 mST	4	Daily	1980–2005
BCSD-CMIP5	SWE	14	Monthly	1975–2000, 2040–2065
NARCCAP	SWE	55	Hourly	1975–2000, 2040–2065
CMIP5	SWE	111	Monthly	1980–2005, 2040–2065

composed of a matrix of five driving GCMs with six RCMs over the Continental United States (CONUS) at 0.5° (55 km) resolution (Mearns et al. 2009). In Phase I (Mearns et al. 2012), pre-2005 simulations (1970–2000) were performed and in Phase II (Mearns et al. 2013), the future projections (2040–2070) were simulated. All of the available RCM-GCM coupled members were utilized to create an ensemble average for the intercomparison.

The Downscaled CMIP3 and CMIP5 Climate and Hydrology Projections dataset consists of an ensemble of model projections using a monthly bias-corrected and spatial disaggregation (BCSD) technique (Maurer et al. 2007; Brekke et al. 2013). For the CMIP5 hydrologic projections (BCSD-CMIP5), the BCSD method was utilized along with the use of the Variable Infiltration Capacity (VIC) hydrologic model, version 4.1.2, to provide 0.125° (14 km) resolution model outputs for both pre-2005 (1970–2000) and future (2040–2070) timeframes. Three of the CESM family ensemble members (i.e., CCSM4, CESM1 BGC, and CESM1 CAM5) were used to create an ensemble average for the model intercomparison.

The North America Land Data Assimilation System Phase 2 (NLDAS) reanalysis dataset was created via the incorporation of observational and model reanalysis datasets into three non-atmosphere coupled land-surface models (i.e., NASA's Mosaic Land Model, NOAA's Noah Land Model, and Princeton's implementation of the VIC Land Model) over the continental US at 0.125° (14 km) resolution for the years 1980–2005 (Xia et al. 2012a, b). Rhoades et al. (2016) showed that the NLDAS ensemble closely approximated the SWE lifecycle (i.e., accumulation, peak timing, and melt rate) of 19 SNOTEL stations in the central Sierra Nevada over 1980–2005, warranting its use in this current analysis.

The Parameter-elevation Relationships on Independent Slopes Model (PRISM) was developed at Oregon State University and consists of a spatially continuous high-resolution (800 m and 4 km) dataset spanning 1970 to present day for the US (Daly et al. 2008). Using a digital elevation model (DEM), 13,000 precipitation and 10,000 temperature observational stations, and several key regional climate indicators (i.e., location, elevation, coastal proximity, topographic orientation and position, vertical atmospheric layer, and terrain slope) the PRISM precipitation and surface temperature dataset was constructed. Of interest to western USA hydroclimatological research in coastal and mountainous regions, PRISM showed great improvement compared to other reanalysis datasets (e.g., Daymet and WorldClim) due to its better characterization of coastal effects, cold air drainage, elevational gradients, inversion layers, and rain shadows in these environments (Daly et al. 2008). Although PRISM is widely regarded and used in the mountain climate community it still has known biases, particularly over the California Sierra Nevada at high-elevations on windward facing slopes, when streamflow observations are utilized as a check on the PRISM total water mass balance (Henn et al. 2016).

It should be cautioned that all of the SWE datasets available have inherent bias. This is due to the use of land-surface models to address the discontinuity of in-situ measurements which only represent a small sub-sample of the total snow covered area. Thus, they should not be viewed as exact "truths". Interestingly, a few new high-resolution spatially continuous observational datasets are becoming more readily available for select mountain regions (in particular the Sierra Nevada and Rockies), but at this time are not yet publicly available. These datasets utilize new techniques including an 50 m resolution airplane lidar measurement (Painter et al. 2016) and a Landsat-era reanalysis product that utilizes the remotely sensed fractional snow cover area along with Bayesian statistical inference techniques to derive a 90 m spatially continuous product (Margulis et al. 2016a, b).

3 Hydroclimate trends in western USA mountain ranges within VR-CESM28

Constraining historically simulated model bias is important in understanding how to best represent the processes governing mountain snowpack within a model. To this end, the VR-CESM28 1980–2005 simulation is assessed against the best available datasets for all western USA mountain ranges regions for total precipitation (PRECT), SWE, and two-meter surface temperature (2 mST). Positive (negative) simulated model biases compared to the 4 km-resolution PRISM data are highlighted in Fig. 4 in blue (red) for daily climate averages of accumulated PRECT and 2 mST. For SWE, several datasets are presented, including the NLDAS three-member ensemble (14 km), the NARCCAP nine-member ensemble (55 km) and the three-member BCSD-CMIP5 ensemble (14 km).

PRISM, used for PRECT and 2 mST, is both a widely used and high quality reanalysis dataset for mountainous regions. Agreement between VR-CESM28 and PRISM is apparent for accumulated daily climate average precipitation in the western USA mountains. A slight positive bias is apparent and consistent across most mountain ranges, but the bias is low, with peak accumulated precipitation of 818 mm for PRISM and 872 mm for VR-CESM28 (+7% bias). Otherwise there is general agreement within the 1980–2005 daily climate normal accumulated precipitation rates for the entire western USA mountain region. Within individual mountain ranges, the Klamath had the highest negative bias (−16%), which can be attributed to the Klamath being the smallest mountain range within the western USA with

rapidly varying orography that is poorly represented even at 28km.

A wide spread among different models is apparent in total simulated SWE, indicative of the difficulty in accurately representing mountainous precipitation deposition and phase as well as the life cycle of mountain snow processes. This variability in simulated vs observed SWE is in part due to the fact that snowpack datasets at sufficiently high resolution and quality are non-existent (notably, models from both the NLDAS and NARCCAP ensemble exhibit unphysically persistent SWE even through the summer season). As highlighted in Rhoades et al. (2016), the NLDAS three-member ensemble was found to be one of the best quality datasets when compared to 19 SNOTEL stations in the Sierra Nevada; however, this may not hold throughout the western USA as each mountain range has a distinct character with respect to aspect, orientation, slope, proximity to the ocean, source precipitation region, and vegetation cover. Thus, it is particularly difficult to assess bias in SWE with no accurate and validated "truth". Nonetheless, it is encouraging to observe that VR-CESM28 appears to fall in the mid-range of the available high-resolution datasets. VR-CESM28 had a peak DJF average accumulation SWE value of 135 mm within the total western USA mountain region, well within the range of values shown by other regional downscaling techniques. The three-member NLDAS ensemble had the lowest peak DJF average accumulation SWE value at 73 mm, followed by the NARCCAP nine-member ensemble at 148 mm and the BCSD-CMIP5 at 172 mm (although this value was derived from monthly, rather than daily averages). As noted by Rhoades et al. (2016), VR-CESM28 also tends to have a early peak accumulation bias associated with an enhanced melt rate leading to total melt occurring too early.

For 2 mST, VR-CESM28 generally shows an enhanced seasonal cycle with increased bias in summer (JJA, max of +1.9 °C) and winter (DJF, min of −2.7 °C) throughout the western USA mountain region, except for the Klamath region where a cold bias is found throughout (min of −2.1 to max of −2.7 °C). For the 2025–2050 period, the VR-CESM28 RCP8.5 simulation still oscillates within the range of bias for PRISM 2 mST, however over the 2075–2100 period temperature values are well outside the 1980–2005 range for simulation bias. This suggests that the climatological signal by end-of-century is beyond the range associated with model bias. The amplified end-of-century warming leads to dramatic reductions in western USA mountain SWE (−69%), with an associated earlier peak snow accumulation and complete melt a month earlier (May), a slightly amplified total accumulated precipitation (+15%), with more rain and less snow (discussed later), and an amplified minimum (+5.8 °C), average (+5.0 °C), and maximum (+4.9 °C) 2 mST.

4 SWE climate change dataset intercomparison for the western USA

To quantify the magnitude and variability of changes in snowpack (SWE) and how VR-CESM28 fits among already widely used downscaling strategies, the VR-CESM28, BCSD-CMIP5, NARCCAP, and CMIP5 climate change datasets were assessed over their overlapping simulation temporal range of 2040–2065 (under RCP8.5) for SWE within the five major western USA mountain ranges. For each of the datasets only CESM derived ensemble members were used, save for NARCCAP where all ensemble members were used. Each of the datasets were separately averaged over their pre-2005 and 2040–2065 periods. Summary statistics across the four global-to-regional downscaling datasets are provided in Table 2 and the pre-2005 vs 2040–2065 percent change summary statistics are provided in Table 3.

The winter season (DJF) climate average for each dataset is plotted in Fig. 5. The datasets all highlight a net-negative change in SWE by 2065, although the magnitudes of change and seasonal variability exhibit some differences. The net change in SWE among the three regional datasets varied from −19% (NARCCAP) to −38% (VR-CESM28). Individual mountain ranges exhibited even more variation in the near-coastal regions (e.g., Cascades and Klamath) with the Klamath showing the most disagreement. The Cascades, Klamath, and Sierra Nevada mean net-SWE loss ranged from −36% (BCSD-CMIP5) to −63% (VR-CESM28), −22% (BCSD-CMIP5) to −74% (VR-CESM28), and −30% (BCSD-CMIP5) to −60% (NARCCAP), with an ensemble mean change of −50, −49, and −44%, respectively. Conversely, more resiliency in snowpack to climate change was seen in the interior mountain ranges (e.g., Rockies and Wasatch and Uinta) across all of the regionally downscaled datasets with net-average changes in SWE ranging from −8% (NARCCAP) to −33% (VR-CESM28) and −21% (NARCCAP) to −41% (BCSD-CMIP5), with an ensemble mean change of −20 and −33%.

The ensemble of CMIP5 simulations poorly characterize the magnitude of 1980–2005 SWE depths (maximum depth of 18.9 mm) and thus highlight an inaccurate and dramatic change (−69%) in SWE totals by 2065. This is largely a consequence of the poor topographic representation which inhibits orographic precipitation and an inaccurate 0 °C isotherm.

Winter season (DJF) variability (standard deviation) for SWE is plotted in Fig. 5 and quantified in Table 3. Compared to the pre-2005 time-frame, most datasets and mountain ranges exhibit a diminished seasonal variability with an overall net-change in SWE variability ranging from +0.3% (NARCCAP) to −20% (BCSD-CMIP5), with an ensemble mean change of −9.4%. This effect was most

Table 2 Summary statistics for the winter season (DJF) average snow water equivalent (SWE) within the western USA mountain ranges

	Climate dataset	Mean (mm)	Standard deviation (mm)	Min (mm)	Lower quartile (mm)	Median (mm)	Upper quartile (mm)	Interquartile range (mm)	Max (mm)	Range (mm)
Western USA mountains										
Pre-2005	VR-CESM28	90.0	5.47	49.7	61.3	83.2	93.8	32.5	163	113
	BCSD-CMIP5	94.7	5.93	22.6	67.0	96.2	114	46.9	197	174
	NARCCAP	106	5.28	60.8	83.3	103	118	35.0	164	103
	CMIP5	2.21	0.70	1.51	1.86	2.19	2.34	0.48	3.69	2.18
	Ensemble	96.8	5.57	44.4	70.5	94.1	109	38.1	174	130
2040–2065	VR-CESM28	56.3	5.07	19.4	39.9	57.5	68.4	28.5	130	111
	BCSD-CMIP5	70.2	4.75	31.8	53.0	68.9	77.7	24.8	113	81.7
	NARCCAP	85.7	5.29	40.1	66.4	81.0	89.9	23.5	155	115
	CMIP5	0.69	0.49	0.36	0.48	0.65	0.74	0.26	1.20	0.83
	Ensemble	70.7	5.04	30.4	53.1	69.1	78.7	25.6	133	102
Cascades										
Pre-2005	VR-CESM28	64.8	7.32	12.1	32.6	47.3	63.8	31.2	220	208
	BCSD-CMIP5	123	7.34	18.1	81.6	117	158	76.1	247	229
	NARCCAP	111	7.06	32.2	73.5	112	137	63.7	201	169
	CMIP5	0.88	0.78	0.18	0.36	0.77	0.98	0.62	2.72	2.55
	Ensemble	99.6	7.24	20.8	62.6	92.0	120	57.0	223	202
2040–2065	VR-CESM28	23.7	5.42	0.45	6.83	16.1	27.3	20.5	146	146
	BCSD-CMIP5	78.1	5.86	23.6	53.2	73.1	94.9	41.7	160	137
	NARCCAP	47.1	5.97	9.47	20.9	36.1	57.8	37.0	162	153
	CMIP5	0.08	0.30	0.01	0.03	0.06	0.09	0.06	0.42	0.41
	Ensemble	49.6	5.75	11.2	27.0	41.8	60.0	33.0	156	145
Klamath										
Pre-2005	VR-CESM28	13.8	3.84	1.33	3.05	7.87	18.1	15.1	63.3	61.9
	BCSD-CMIP5	61.7	6.13	10.7	34.1	59.5	78.0	43.9	151	140
	NARCCAP	50.9	5.16	8.79	24.9	54.8	58.7	33.7	121	112
	CMIP5	0.24	0.46	0.02	0.09	0.14	0.28	0.19	0.80	0.77
	Ensemble	42.2	5.13	6.94	20.7	40.7	51.6	30.9	112	105
2040–2065	VR-CESM28	3.58	2.20	0.09	0.64	2.28	3.71	3.07	23.6	23.5
	BCSD-CMIP5	47.9	5.53	9.37	18.2	38.8	65.2	47.0	113	104
	NARCCAP	13.5	3.67	1.26	3.66	8.66	14.7	11.0	51.4	50.1
	CMIP5	0.01	0.12	0.00	0.01	0.01	0.01	0.01	0.06	0.06
	Ensemble	21.7	4.04	3.57	7.50	16.5	27.9	20.4	62.7	59.1

Table 2 (continued)

	Climate dataset	Mean (mm)	Standard deviation (mm)	Min (mm)	Lower quartile (mm)	Median (mm)	Upper quartile (mm)	Interquartile range (mm)	Max (mm)	Range (mm)
Rockies										
Pre-2005	VR-CESM28	102	5.65	56.2	74.1	94.5	125	51.1	159	103
	BCSD-CMIP5	91.3	5.71	26.7	71.1	93.0	103	31.7	197	171
	NARCCAP	114	5.29	64.9	92.3	112	127	34.5	183	118
	CMIP5	2.71	0.81	1.80	2.29	2.56	2.83	0.54	4.76	2.96
	Ensemble	102.2	5.55	49.3	79.2	99.7	118	39.1	180	131
2040–2065	VR-CESM28	68.2	5.37	21.5	50.8	74.3	79.8	29.0	140	119
	BCSD-CMIP5	71.1	4.60	31.4	58.1	68.5	81.7	23.5	115	83.8
	NARCCAP	105	5.49	52.3	87.5	104	114	26.0	180	127
	CMIP5	0.88	0.55	0.46	0.62	0.83	0.94	0.31	1.45	0.99
	Ensemble	81.5	5.17	35.1	65.5	82.4	91.7	26.2	145	110
Sierra Nevada										
Pre-2005	VR-CESM28	79.4	6.98	2.70	32.8	86.9	106	72.7	203	200
	BCSD-CMIP5	119	8.92	11.5	45.7	110	158	112	264	252
	NARCCAP	63.8	5.92	13.3	32.0	54.3	81.8	49.8	128	115
	CMIP5	0.48	0.62	0.04	0.22	0.34	0.58	0.36	1.64	1.60
	Ensemble	87.4	7.38	9.17	36.8	83.8	115	78.1	198	189
2040–2065	VR-CESM28	38.6	6.22	2.61	10.7	25.3	33.5	22.8	160	157
	BCSD-CMIP5	83.4	6.47	17.8	41.9	81.4	108	66.5	176	158
	NARCCAP	25.2	4.74	3.75	5.81	19.2	26.2	20.4	89.7	86.0
	CMIP5	0.03	0.19	0.00	0.01	0.02	0.04	0.03	0.17	0.17
	Ensemble	49.1	5.86	8.07	19.5	42.0	56.0	36.5	142	134
Wasatch and Uinta										
Pre-2005	VR-CESM28	90.6	5.77	25.7	64.9	89.4	99.2	34.3	175	149
	BCSD-CMIP5	74.6	6.51	4.84	41.3	64.2	101	59.4	181	176
	NARCCAP	88.8	5.65	38.2	64.6	88.4	106	41.2	156	117
	CMIP5	1.12	0.66	0.43	0.86	1.09	1.15	0.28	2.45	2.02
	Ensemble	84.7	5.99	22.9	56.9	80.6	102	45.0	171	148
2040–2065	VR-CESM28	56.3	5.52	13.5	27.9	56.3	65.5	37.6	115	102
	BCSD-CMIP5	44.4	4.45	12.0	28.0	41.9	56.3	28.3	82.9	70.9
	NARCCAP	69.8	5.73	21.1	40.9	64.4	87.9	46.9	157	136
	CMIP5	0.24	0.33	0.08	0.15	0.20	0.30	0.15	0.48	0.40
	Ensemble	56.8	5.26	15.5	32.3	54.2	69.9	37.6	118	103

Note that BCSD-CMIP5 was capped at 1500 mm due to anomalously high SWE values in select grid points (e.g., Cascades). The ensemble value is the average of the three-regionally downscaled datasets (i.e., VR-CESM28, BCSD-CMIP5, and NARCCAP)

Table 3 Pre-2005 vs 2040–2065 percent change for the winter season (DJF) average snow water equivalent (SWE) within the western USA mountain ranges

	Climate dataset	Mean (% change)	Standard deviation (% change)	Min (% change)	Lower quartile (% change)	Median (% change)	Upper quartile (% change)	Interquartile range (% change)	Max (% change)	Range (mm)
Western USA mountains										
Pre-2005 vs 2040–2065	VR-CESM28	−37.5	−7.25	−60.9	−34.9	−30.9	−27.1	−12.3	−20.1	−2.20
	BCSD-CMIP5	−25.9	−19.9	40.6	−20.9	−28.4	−31.7	−47.2	−42.3	−53.0
	NARCCAP	−18.9	0.28	−34.0	−20.4	−21.2	−24.0	−32.8	−5.54	11.3
	CMIP5	−68.6	−29.7	−75.9	−74.1	−70.3	−68.2	−45.0	−67.5	−61.7
	Ensemble	−26.9	−9.38	−31.4	−24.7	−26.5	−27.6	−32.9	−23.9	−21.3
Cascades										
Pre-2005 vs 2040–2065	VR-CESM28	−63.4	−26.0	−96.3	−79.0	−66.0	−57.3	−34.5	−33.4	−29.8
	BCSD-CMIP5	−36.3	−20.1	30.5	−34.8	−37.3	−39.8	−45.2	−35.2	−40.4
	NARCCAP	−57.7	−15.4	−70.6	−71.6	−67.7	−57.9	−42.0	−19.4	−9.60
	CMIP5	−90.6	−62.0	−94.5	−91.4	−91.7	−90.7	−90.3	−84.7	−84.0
	Ensemble	−50.2	−20.5	−46.3	−56.9	−54.6	−49.8	−42.1	−29.9	−28.2
Klamath										
Pre-2005 vs 2040–2065	VR-CESM28	−74.1	−42.8	−93.3	−79.1	−71.0	−79.6	−79.6	−62.6	−62.0
	BCSD-CMIP5	−22.3	−9.82	−12.3	−46.5	−34.8	−16.4	7.02	−24.9	−25.9
	NARCCAP	−73.5	−28.8	−85.6	−85.3	−84.4	−75.0	−67.3	−57.5	−55.3
	CMIP5	−94.9	−74.7	−98.2	−98.2	−95.2	−94.7	−93.1	−92.8	−92.6
	Ensemble	−48.6	−21.3	−48.5	−63.7	−59.4	−46.0	−34.1	−43.8	−43.5
Rockies										
Pre-2005 vs 2040–2065	VR-CESM28	−33.0	−4.94	−61.8	−31.4	−21.4	−36.3	−43.3	−12.0	15.2
	BCSD-CMIP5	−22.1	−19.4	17.7	−18.3	−26.3	−20.5	−25.7	−41.6	−50.9
	NARCCAP	−7.50	3.81	−19.5	−5.12	−6.63	−10.4	−24.5	−1.91	7.72
	CMIP5	−67.5	−32.2	−74.2	−72.8	−67.4	−66.9	−42.0	−69.5	−66.7
	Ensemble	−20.3	−6.93	−28.9	−17.3	−17.4	−22.5	−33.0	−19.4	−15.9
Sierra Nevada										
Pre-2005 vs 2040–2065	VR-CESM28	−51.4	−10.8	−3.53	−67.3	−70.9	−68.2	−68.7	−21.5	−21.7
	BCSD-CMIP5	−30.1	−27.5	55.6	−8.20	−26.0	−31.2	−40.6	−33.3	−37.4
	NARCCAP	−60.4	−20.0	−71.9	−81.8	−64.6	−68.0	−59.1	−30.0	−25.1
	CMIP5	−93.1	−69.7	−98.9	−96.2	−93.1	−93.2	−91.4	−89.8	−89.6
	Ensemble	−43.9	−20.6	−12.1	−47.1	−49.9	−51.3	−53.2	−28.6	−29.4
Wasatch and Uinta										
Pre-2005 vs 2040–2065	VR-CESM28	−37.8	−4.29	−47.6	−57.0	−37.0	−34.0	9.54	−34.1	−31.8
	BCSD-CMIP5	−40.6	−31.7	148.0	−32.1	−34.8	−44.0	−52.3	−54.3	−59.8
	NARCCAP	−21.3	1.44	−44.9	−36.6	−27.1	−16.9	13.9	0.76	15.6
	CMIP5	−78.6	−49.7	−81.3	−82.5	−81.3	−74.1	−48.5	−80.4	−80.2
	Ensemble	−32.9	−12.1	−32.4	−43.3	−32.8	−31.4	−16.4	−30.6	−30.4

The ensemble value is the average of the three-regionally downscaled datasets (i.e., VR-CESM28, BCSD-CMIP5, and NARCCAP)

pronounced in coastal ranges, especially in the Klamath which exhibited a net-change of −9.8% (BCSD-CMIP5) to −43% (VR-CESM28). This is explained by the negative shift in maximum SWE coupled with an overall collapse of the lower-to-upper quartile ranges in most of the regional downscaling datasets, highlighted in the DJF seasonal averages in Fig. 6. To further quantify this, uncentered Pearson pattern correlations were computed for the ratio of the DJF climate average and seasonal variability for pre-2005 and 2040–2065 for the entire western USA mountain region. Across all datasets, a high-correlation (>0.91) was found for the aforementioned ratio, indicating that a decrease in the climate average DJF SWE corresponds to a decrease in the seasonal variability (i.e., collapse of the interquantile ranges).

5 DJF climate trends in snowfall, snow cover, SWE and 2 mST in VR-CESM

Changes in SWE are a function of a number of topographically dependent variables including snowfall, snow cover, and 2 mST (and their associated variabilities). To better understand the character of the western USA snowpack, the impact of climate change on these quantities must also be understood. Summary statistics for these quantities from VR-CESM28 are given in Table 4 and are only representative of the mountainous regions in Fig. 3.

An assessment of the statistical significance ($p = 0.05$) of the VR-CESM28 simulated winter (DJF) season frequency change for the 1980–2005 compared to the RCP8.5 2025–2050 and 2075–2100 simulation results within the western USA mountain region across all hydroclimate variables was performed using the Wilcoxon–Mann–Whitney rank-sum test. This statistical significance test is useful for data that may not be normally distributed and helps to identify when significant changes associated with RCP8.5 begin to take effect on the simulated results. As can be seen in Table 4, significant ($p < 0.05$) changes from 1980 to 2005 PDFs for each of the hydroclimate variables are varied in the 2025–2050 results, but are unanimous in the 2075–2100 results across all mountain ranges. As expected, this implies a significantly more pronounced climate change signal by 2075–2100 compared with 2025–2050.

DJF climatological averages for snowpack variables are plotted in Fig. 7 for 1980–2005, 2025–2050, and 2075–2100 under the RCP8.5 scenario in VR-CESM28. Additionally, the DJF seasonal average summary statistics are provided in Table 4 which represent only the mountainous regions depicted in Fig. 3. The climatological anomalies (difference between 1980–2005 and post–2025) are plotted in the bottom two rows. Clear trends are seen throughout the western USA for all of the hydroclimate variables, with an amplified trend by 2075–2100. For snowfall (d, e), a small decrease (−4%) is projected for the entire western USA mountain region by 2025–2050, with both positive (Intermountain West) and negative (Coastal Ranges) tendencies. By 2075–2100, the climate change signal is more apparent with an average decrease of −30% in total western USA mountain snowfall that is amplified along the Pacific coast due to a precipitation transition from snow-to-rain. This net decrease in snowfall helps to explain the substantial decrease in both snow cover (i, j) and SWE (n, o). As with snowfall, snow cover (−10%) and SWE (−25%) only exhibit a weak response to climate change through 2025–2050; however, by 2075–2100 average snow cover decreases by nearly half (−44%) and SWE by two-thirds (−69%) throughout the study domain. These changes are associated with an average increase in western USA 2 mST anomalies (s, t) of +1.3 °C over the 2025–2050 period and +5.0 °C over the 2075–2100 period. Notably, there is a clear spatial signal in the surface temperature anomaly, with larger increases in average temperature at high elevation associated with elevation-dependent warming (discussed later).

An expected shift in precipitation phase from snow to rain has been posited throughout the literature due to climate change induced increases in air temperature (Bales et al. 2006; Berghuijs et al. 2014; Klos et al. 2014; Lute et al. 2015). This result is apparent in the VR-CESM28 simulations (Fig. 8), which exhibit a clear shift from snow-to-rain (a–e) along with more wet snow deposition (f–j) (i.e., decreased liquid-to-snow ratio). The snow-to-rain plots (a–c) are DJF climate average ratios of snowfall over total precipitation and the liquid-to-snow ratio plots (f–h) are DJF climate average ratios of snow water equivalent to snow depth. 1980–2005 DJF climate average VR-CESM28 total precipitation was 3.5 mm/day and snowfall was 2.3 mm/day, but by 2025–2050 (2075–2100) DJF climate average total precipitation increased to 3.6 mm/day (4.00 mm/day) and DJF climate average snowfall decreased to 2.2 mm/day (1.6 mm/day). The alteration in the precipitation phase within the western USA mountainous region resulted in a −4% (−24%) drop in the snow-to-rain ratio by 2025–2050 (2075–2100) coupled with a mean increase in total precipitation of +7% (+20%). The statistical significance of the change in snow-to-rain and liquid-to-snow ratios for 2025–2050 were mixed in all of the mountain ranges; however, by 2075–2100 the statistical significance in these changes become unanimous across all mountain ranges at the $p = 0.05$ and $p = 0.01$ threshold. Sensitivity of coastal ranges to precipitation phase alterations was evident. By 2075–2100, both the Cascades and Sierra Nevada showed a drop of −32 and −30% in their snow-to-rain ratios. A slightly wetter snowpack emerges as the DJF climate average liquid-to-snow ratio drops by −3%, with a

Table 4 Winter season (DJF) average anomalies within western USA mountain ranges for RCP8.5 2025–2050 and 2075–2100 VR-CESM28 simulations

Winter season anomalies	Wilcoxon rank-sum test p value ($p = 0.05$)	Mean	Standard deviation	Min	Lower quartile	Median	Upper quartile	Inter-quartile range	Max
Western USA mountains									
Snowfall (% change)									
2025–2050	0.577 (False)	−4.39	9.53	−18.9	−14.6	1.44	−1.88	12.7	21.8
2075–2100	1.69×10^{-4} (True)	−29.8	1.22	−43.5	−39.1	−35.0	−13.9	25.2	−24.4
Snow cover (% change)									
2025–2050	0.0371 (True)	−10.2	29.0	−39.4	−11.7	−9.44	−4.47	7.23	−0.28
2075–2100	3.16×10^{-14} (True)	−44.2	22.7	−68.3	−68.3	−42.9	−35.6	17.0	−31.8
Snow water equivalent (% change)									
2025–2050	3.97×10^{-3} (True)	−24.9	1.81	−58.5	−29.2	−19.7	−20.1	9.15	3.63
2075–2100	4.30×10^{-12} (True)	−68.9	−23.4	−88.3	−79.0	−70.8	−57.7	21.3	−55.7
Surface temperature [anomaly (°C)]									
2025–2050	0.0320 (True)	1.31	0.21	0.76	0.61	0.75	1.67	1.05	2.34
2075–2100	1.90×10^{-13} (True)	5.03	0.01	5.83	4.85	4.65	5.08	0.23	4.91
Cascades									
Snowfall (% change)									
2025–2050	0.289 (False)	−10.7	8.68	−34.1	−32.1	−0.84	7.98	40.1	14.5
2075–2100	6.97×10^{-8} (True)	−54.9	−8.60	−87.0	−72.6	−56.3	−44.9	27.7	−40.9
Snow cover (% change)									
2025–2050	0.0247 (True)	−20.3	4.88	−55.0	−33.5	−17.1	−10.5	23.0	−5.33
2075–2100	3.09×10^{-12} (True)	−71.5	−18.5	−94.0	−82.4	−71.5	−68.3	14.1	−51.0
Snow water equivalent (% change)									
2025–2050	1.86×10^{-3} (True)	−44.3	−11.8	−82.3	−68.7	−45.8	−39.9	28.8	−4.11
2075–2100	4.30×10^{-12} (True)	−90.1	−61.0	−99.0	−96.3	−92.6	−90.1	6.21	−83.4
Surface temperature [anomaly (°C)]									
2025–2050	0.108 (False)	0.91	0.04	1.25	0.64	0.76	0.41	−0.23	1.23
2075–2100	1.06×10^{-12} (True)	4.17	−0.12	4.96	4.09	4.02	3.89	−0.19	3.38
Klamath									
Snowfall (% change)									
2025–2050	0.271 (False)	−18.3	−5.91	−31.7	0.26	−19.0	−13.9	−14.2	4.64
2075–2100	4.29×10^{-11} (True)	−78.3	−42.2	−95.0	−87.6	−78.6	−77.0	10.6	−72.6
Snow cover (% change)									
2025–2050	0.0494 (True)	−32.7	−20.2	−62.5	−20.9	−19.3	−34.9	−14.0	−21.4
2075–2100	1.54×10^{-12} (True)	−87.9	−57.6	−99.5	−94.2	−87.6	−87.7	6.43	−84.3
Snow water equivalent (% change)									
2025–2050	0.0741 (False)	−43.1	−7.31	−79.6	−30.2	−47.8	−49.4	−19.2	2.49
2075–2100	1.54×10^{-13} (True)	−96.1	−78.8	−99.9	−97.6	−96.1	−97.0	0.61	−96.3
Surface temperature [anomaly (°C)]									
2025–2050	0.0679 (False)	0.82	0.02	1.56	1.23	0.23	0.60	−0.63	1.22
2075–2100	1.90×10^{-13} (True)	3.69	−0.06	4.48	3.84	3.47	3.59	−0.25	3.21
Rockies									
Snowfall (% change)									
2025–2050	0.672 (False)	−2.29	4.56	−3.59	−6.04	1.41	1.60	7.65	8.28

Table 4 (continued)

Winter season anomalies	Wilcoxon rank-sum test p value ($p = 0.05$)	Mean	Standard deviation	Min	Lower quartile	Median	Upper quartile	Inter-quartile range	Max
2075–2100	9.01×10^{-3} (True)	−16.4	6.03	−23.9	−23.3	−19.9	−6.87	16.5	−9.22
Snow cove (% change)									
2025–2050	0.0621 (False)	−7.72	42.9	−42.5	−9.66	−8.25	−3.64	6.02	0.34
2075–2100	1.58×10^{-14} (True)	−38.1	47.2	−67.4	−48.8	−38.1	−27.6	21.2	−27.5
Snow water equivalent (% change)									
2025–2050	0.0108 (True)	−22.8	−3.78	−61.8	−26.2	−17.5	−30.8	−4.59	−5.29
2075–2100	4.29×10^{-11} (True)	−64.9	−18.0	−85.7	−77.1	−65.3	−58.6	18.6	−42.6
Surface temperature [anomaly (°C)]									
2025–2050	0.0371 (True)	1.41	0.26	0.95	0.75	0.60	1.99	1.24	2.36
2075–2100	1.90×10^{-13} (True)	5.32	0.05	6.41	4.75	4.91	5.82	1.07	5.46
Sierra Nevada									
Snowfall (% change)									
2025–2050	0.603 (False)	−2.64	11.7	−65.7	14.1	−15.5	−5.69	−19.8	70.0
2075–2100	1.83×10^{-5} (True)	−54.8	−20.1	−68.0	−62.1	−59.6	−51.0	11.1	−34.0
Snow cover (% change)									
2025–2050	0.0494 (True)	−18.9	1.53	−71.9	−23.0	−25.7	−19.0	4.02	8.18
2075–2100	4.03×10^{-9} (True)	−66.8	−17.5	−89.5	−78.1	−69.6	−63.8	14.3	−43.1
Snow water equivalen (% change)									
2025–2050	0.0994 (False)	−18.7	24.9	−83.5	−34.1	−52.6	−44.3	−10.2	73.1
2075–2100	1.70×10^{-7} (True)	−83.3	−33.8	−94.6	−96.1	−94.2	−86.6	9.46	−53.8
Surface temperature [anomaly (°C)]									
2025–2050	0.0353 (True)	1.06	0.10	1.46	0.92	0.73	0.75	−0.17	3.18
2075–2100	4.75×10^{-13} (True)	4.18	0.00	4.72	3.91	3.95	4.39	0.48	4.21
Wasatch and Uinta									
Snowfall (% change)									
2025–2050	0.893 (False)	1.23	10.7	−61.2	−5.07	−1.07	0.95	6.02	27.3
2075–2100	5.50×10^{-3} (True)	−22.8	4.12	−24.5	−29.5	−30.5	−33.7	−4.21	6.50
Snow cover (% change)									
2025–2050	0.0472 (True)	−13.1	14.6	−64.4	−18.6	−14.1	−17.9	0.73	4.28
2075–2100	1.04×10^{-9} (True)	−51.0	8.10	−80.8	−61.7	−54.9	−49.8	11.9	−16.7
Snow water equivalent (% change)									
2025–2050	0.0136 (True)	−24.1	14.8	−67.5	−37.5	−35.0	−13.5	24.0	19.1
2075–2100	4.03×10^{-9} (True)	−70.3	−14.4	−86.8	−85.9	−80.2	−65.9	20.0	−44.8
Surface temperature [anomaly (°C)]									
2025–2050	7.51×10^{-3} (True)	1.83	0.20	1.30	1.45	1.09	2.04	0.59	2.70
2075–2100	1.06×10^{-12} (True)	5.83	0.02	5.90	5.73	5.68	6.09	0.36	4.75

The Wilcoxon rank-sum test p values are also given with a true (false) indication if the p value is below (above) the 0.05 significance level

decrease of −5% (lower quartile) to −11% (minimum) in parts of the study domain by 2075–2100.

5.1 Winter season variability in 2 mST, snowfall, SWE, and snow cover

Winter season snowpack interannual variability plays a crucial role in water resource planning in the western USA. An understanding of this variability is required to ensure sufficient water availability during inevitable drought periods. The DJF interannual variability from VR-CESM28 for the four hydroclimate variables of interest is apparent in Fig. 9 for several of the western USA mountainous regions as a Hovmöller diagram of DJF latitudinal averages. The Hovmöller diagrams are useful in characterizing not only the seasonal variability, but the latitudinal dependence of these changes too. The anomalous deviations from the 1980–2005 DJF average are represented in each figure with the 1980–2005 time period on the left, a gap filled 2005–2025 in the middle (not simulated), and, finally, the RCP8.5 scenario results from 2025 to 2100 on the right. Anomalously high (low) DJF seasons compared to the 1980–2005 climate average are represented via blue (red), whereas the 2 mST anomaly trend colors are flipped for reader intuition.

In Fig. 9, historical (1980–2005) hydroclimate trends within the region oscillate from season-to-season about the mean with even distributions of high and low events. As the RCP8.5 climate change signal intensifies by the mid-to-end of century, a clear reduction in anomalously high winter season snowfall, snow cover, and SWE occurs with a coupled increase in anomalously high 2 mST. Notably, by the 2050s anomalously high winter season snowfall, snow cover, and SWE become effectively non-existent with anomalously high 2mST (+3 to +6 °C) becoming the new normal. The anomalously high 2 mST in the western USA mountainous region is correlated with the demise of snow cover.

5.2 Elevation-dependent warming

Elevation-dependent warming is associated with an increased warming signal in mountain regions due to a combination of the snow-albedo feedback, changes in vertical humidity profiles of the lower atmosphere, and/or cloud-feedback processes (Group et al. 2015). To understand the character of this phenomena within our simulations, Figs. 10 and 11 show 250 m interval elevational profile plots of the DJF climate average and 500 m elevational band trends for the DJF seasonal average time-series, respectively. For the 250 m elevational profile plots, three selected mountain ranges [Cascades (e–h), Rockies (i–l), and Sierra Nevada (m–p)] are included with the total western USA mountainous region (a–d). These three mountains were selected as they represent the major mountainous regions for water management and each spans the largest range of latitudes within the western USA. Additionally, the 500 m elevational band summary statistics were compiled in Table 5, along with the standardized regression coefficients, for each of the time-series and hydroclimate variable. Historically, it is the case that elevations with maximum snowfall often do not co-locate with maximum snow cover. In fact, western USA snowfall seems to be most pronounced around an elevation of ~ 1000 m (except for the Sierra Nevada), whereas snow cover increases approximately monotonically with elevation. The California Sierra Nevada trends may differ from the other mountain ranges of the western USA as it has a unique combination of atmosphere-ocean factors which could alter precipitation phase and deposition location. These features include its close proximity to the ocean, high perpendicularity to the coastline, highest elevations in the conterminous United States and precipitation trends dependent on the semi-permanent large-scale meteorological pattern (e.g., Aleutian Low), association with extreme meteorology (e.g., atmospheric rivers), and, in the southern portion, precipitation that is highly dependent on teleconnection patterns (e.g., the ENSO and the North American Monsoon).

Several hydroclimatic trends further emerge from this dataset. Examining Fig. 10, although it is clear that the RCP8.5 climate change signal is much more apparent in the 2075–2100 DJF climate average than the 2025–2050 period, the actual impacts are not distributed uniformly across elevation categories. Throughout most of the western USA, only elevations below 2000 m exhibit a clear climate signal with respect to snowfall (again except for the Sierra Nevada). Over the entire western USA mountainous region (a), peak average snowfall at 1250 m elevation is diminished from 3.16 mm/day (1980–2005) to 2.87 mm/day (2025–2050), or −9%, and finally to 1.85 mm/day, or −41% (2075–2100). Interestingly, peak snowfall elevation (1250 m) is maintained across all of the time-series in the total western USA mountainous region; however, in 2075–2100 the peak snowfall magnitude is maintained over a broader range of elevation bands with a slight increase in snowfall at higher elevations compared to the 1980–2005 and 2025–2100 time periods. In response to the decrease in low-elevation snowfall, snow cover and SWE also decrease dramatically below ~2000 m. Higher elevations are also impacted by warmer surface temperatures which reduce snow cover and SWE, but these regions appear to be more strongly buffered against climate change.

Elevation-dependent warming is also apparent in the simulations as a consequence of the snow-albedo feedback. Namely, an increased DJF climate average 2 mST warming

Table 5 VR-CESM28 simulated winter season (DJF) average 500 m elevational anomalies within the total western USA mountain range for 1980–2005 and 2025–2100 under the RCP8.5 climate forcing

Average winter anomaly	Elevation (m)	Min	Mean	Max	Interquartile range	Standardized regression coefficient
Snowfall (% change)						
1980–2005 (2025–2100)	>500	−56.3 (−94.5)	0.00 (−50.1)	113 (91.8)	42.0 (47.2)	−0.03 (−0.64)
	>1000	−36.1 (−78.8)	0.00 (−29.2)	51.5 (90.7)	23.0 (43.0)	−0.20 (−0.50)
	>1500	−32.4 (−50.4)	0.00 (−12.6)	30.3 (61.1)	29.7 (36.8)	−0.30 (−0.36)
	>2000	−35.1 (−48.4)	0.00 (−1.92)	38.6 (59.7)	28.6 (36.0)	−0.25 (−0.20)
	>2500	−37.4 (−48.8)	0.00 (5.88)	62.4 (70.9)	22.3 (29.7)	−0.15 (−0.04)
	>3000	−39.5 (−54.9)	0.00 (7.88)	78.9 (93.0)	25.1 (43.2)	−0.05 (0.04)
Snow cover (% change)						
1980–2005 (2025–2100)	>500	−73.3 (−97.7)	0.00 (−58.7)	97.4 (43.6)	61.7 (53.5)	0.10 (−0.67)
	>1000	−35.9 (−89.2)	0.00 (−39.8)	37.8 (35.8)	27.3 (47.0)	−0.04 (−0.66)
	>1500	−32.9 (−82.9)	0.00 (−33.0)	23.1 (32.2)	22.0 (36.0)	−0.17 (−0.61)
	>2000	−24.1 (−73.5)	0.00 (−26.3)	22.2 (23.5)	15.3 (33.1)	−0.14 (−0.61)
	>2500	−32.2 (−65.8)	0.00 (−20.6)	28.4 (25.4)	15.3 (27.2)	−0.20 (−0.53)
	>3000	−24.0 (−66.3)	0.00 (−14.3)	11.9 (13.5)	12.1 (21.3)	−0.14 (−0.44)
SWE (% change)						
1980–2005 (2025–2100)	>500	−90.2 (−99.8)	0.00 (−74.7)	230 (102)	70.7 (32.2)	0.01 (−0.50)
	>1000	−64.3 (−99.1)	0.00 (−62.9)	147 (174)	42.3 (43.0)	−0.06 (−0.53)
	>1500	−63.9 (−97.2)	0.00 (−51.0)	88.0 (120)	54.2 (41.0)	−0.14 (−0.54)
	>2000	−54.4 (−92.3)	0.00 (−42.6)	69.0 (86.5)	34.5 (48.7)	−0.04 (−0.58)
	>2500	−54.2 (−85.0)	0.00 (−32.1)	141 (99.2)	42.2 (52.9)	0.01 (−0.46)
	>3000	−52.2 (−88.7)	0.00 (−17.5)	123 (220)	51.9 (52.9)	0.08 (−0.32)
2 mST [Anomaly (°C)]						
1980–2005 (2025–2100)	>500	−2.95 (−0.76)	0.00 (0.97)	3.05 (2.35)	1.69 (1.18)	0.02 (0.66)
	>1000	−3.29 (−2.38)	0.00 (2.85)	3.11 (7.01)	1.65 (3.58)	0.04 (0.63)
	>1500	−3.15 (−2.78)	0.00 (3.29)	3.23 (8.28)	1.87 (3.76)	0.13 (0.61)
	>2000	−3.60 (−2.33)	0.00 (3.81)	3.71 (9.25)	1.39 (4.32)	0.21 (0.62)
	>2500	−3.36 (−1.63)	0.00 (3.55)	3.70 (8.85)	1.48 (3.52)	0.28 (0.62)
	>3000	−2.73 (−1.67)	0.00 (3.50)	3.74 (9.43)	1.33 (3.54)	0.29 (0.60)

emerges by 2075–2100 (Fig. 10d) which is maximal around an elevation of 2000 m (Fig. 11). The freezing line (highlighted with a dotted line at 273.14 K) shifts upwards in elevation from 750 to 1500 m from 1980–2005 to 2075–2100 within the total western USA mountainous region. However, the elevation-dependent sensitivity to increases in 2 mST is not uniformly distributed. Interior mountain ranges (e.g., Rockies) maintain their freezing line at elevations that the coastal ranges (e.g., Cascades) showed an increased sensitivity to warming. For example, the 1980–2005 freezing line moved up in the Cascades from 750 to 1750 m, in the Rockies from 500 to 1000 m, and in the Sierra Nevada from 1500 to 2250 m by 2075–2100. By 2075–2100, the Cascades' DJF climate average 2 mST was above the freezing line throughout all elevations, with the Sierra Nevada showing a similar trend save for the highest elevation class.

The upslope shift in elevation of the freezing line directly impacted the snow covered area and, importantly, the stored water content (SWE) of the snowpack. From 1980–2005 to 2075–2100, the average accumulated SWE (i.e., stored water content or the area under the curve) is diminished by −21% by 2025–2050 and −63% by 2075–2100 within the total western USA mountain region. Further, 1980–2005 accumulated SWE diminished in the Cascades by −43% (−89%), in the Rockies by −22% (−63%), and in the Sierra Nevada by −18% (−82%) within 2025–2050 (2075–2100).

The 500 m elevational band winter (DJF) climate average anomaly trends for 1980–2005 and 2025–2100 are plotted in Fig. 11 and statistically summarized in Table 5. As anticipated with 2 mST increases due to climate change, the largest decreases found in the VR-CESM28 simulations from 2025 to 2100 were at lower elevations, likely due to the phase shift from snow-to-rain seen in Fig. 8 and upward shift in freezing line elevation. Resiliency of snowfall to climate change was shown at higher elevations starting at

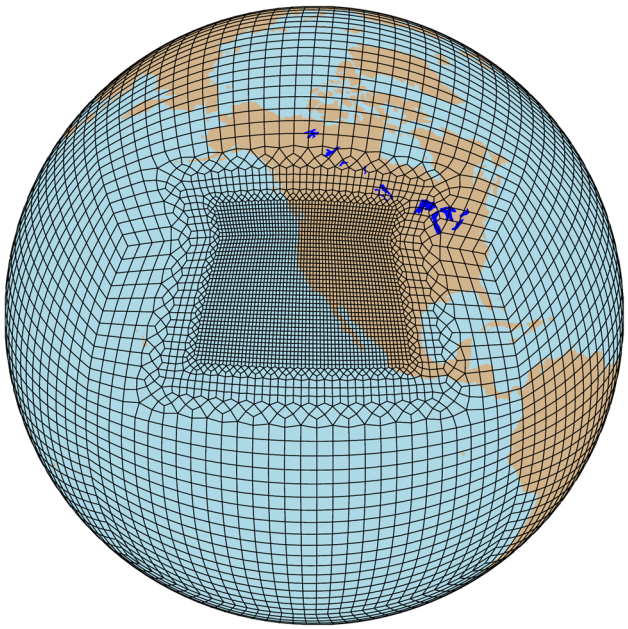

Fig. 1 The VR-CESM grid used for this study utilized a quasi-uniform 111 km (1°) base-resolution in a cubed-sphere grid structure. The smooth VR refinement region is depicted via the convex polygons with the highest grid resolution of 28 km (0.25 °) over the Eastern Pacific and the western USA

around 2000–2500 m where nominal positive or negative trends occurred. Elevational trends indicated a nonlinear negative change in snowfall of −10.7% from 2000 to 1500 m, −16.6% from 1500 to 1000 m, and, finally, −20.9% from 1000 to 500 m. This was further shown in the standardized regression coefficients which steadily decreased towards negative one with every 500 m decent with coefficients ranging from 0.04 (>3000 m) to −0.64 (500–1000 m).

As shown in Fig. 11b, c, from 2025 to 2100 a clear negative trend in SWE and snow cover, regardless of elevation, was found. This is further shown in the standardized regression coefficients in Table 5. Interestingly, when compared to snowfall, both SWE and snow cover more linearly decreased downslope. Winter season average snow cover trends indicated a −5.7%/500 m to −6.8%/500 m, save for the change from 1000 to 500 m of −18.9%/500 m, and SWE trends showed a −11%/500 m to −15%/500 m.

Anti-correlated to the aforementioned trends, average winter season 2 mST anomalies showed a steady increase and plateau upslope in the western USA mountain region (Fig. 11). Average winter season 2 mST anomalies highlighted a +0.97 °C from 500 to 1000 m and then a more rapid increase of +2.85 to +3.81 °C from 1000 to >3000 m. Further, the average maximum 2 mST anomaly at the 500–1000m elevation band was +2.35 °C; whereas, the 1000 m to >3000m ranged from +7.01 to +9.43 °C. As shown in Table 5, the magnitude of the interquantile ranges (i.e., an indication of seasonal variability) for 2 mST increased by 101–210% from 1980–2005 to 2025–2100 from 1000 to >3000 m and decreased by 30% from 500 to 1000 m.

6 Discussion and conclusion

Water managers, particularly in the western USA, have been increasingly demanding accurate projections of mountain snowpack in the coming century. To address this need, this paper has leveraged the highest quality publicly available snowpack projections (e.g., BCSD-CMIP5, CMIP5, and NARCCAP) to understand historical and projected 21st-century western USA mountain snowpack, augmented by cutting-edge climate simulations of the coming century

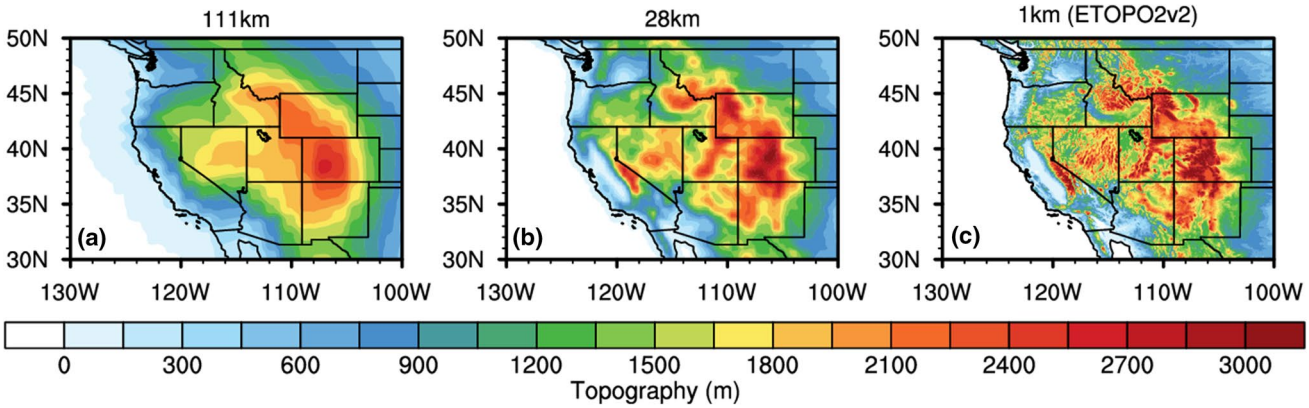

Fig. 2 Comparison of topographical distributions between **a** standard uniform-resolution 111 km (1°) CESM and **b** VR-CESM 28 km (0.25°) to **c** the satellite derived ETOPO2v2 1 km (2′) dataset

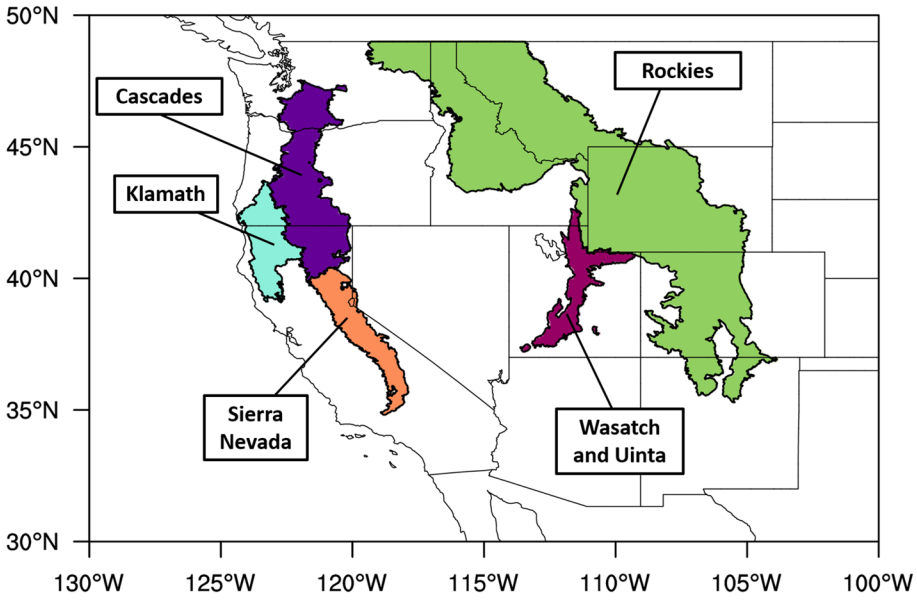

Fig. 3 The five EPA Ecoregion III sub-regions used in this assessment, delineated by *color* and *emboldened lines*

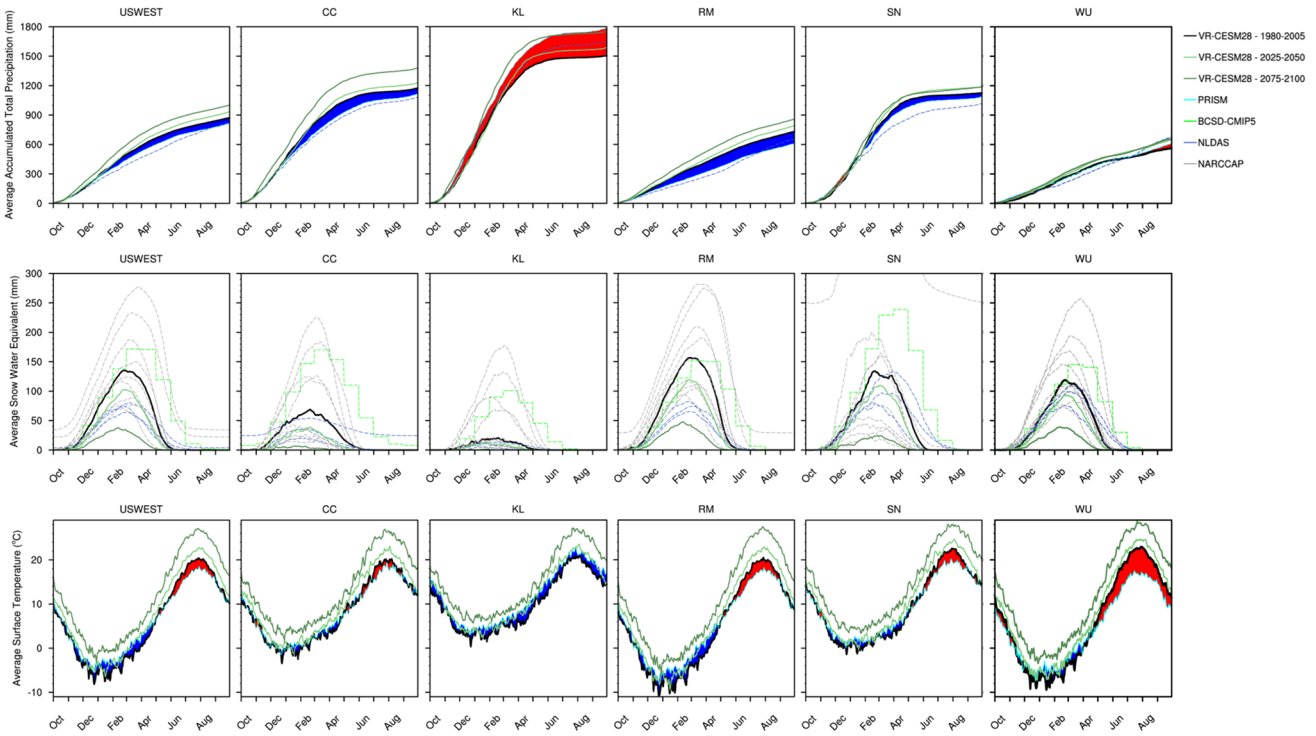

Fig. 4 VR-CESM28 climate daily average (pre-2005) values for accumulated precipitation (*top*), SWE (*center*), and two-meter surface temperature (*bottom*) against PRISM, BCSD-CMIP5, NLDAS, and NARCCAP within the total western USA mountain ranges (*first column*) and all of the individual mountain ranges. VR-CESM28 model bias is highlighted in *blue* (*red*) for over (under) accumulation in precipitation and *red* (*blue*) for positive (negative) 2-m surface temperature. VR-CESM28 climate daily averages for RCP8.5 2025–2050 and 2075–2100 results are superimposed over the 1980–2005 results in *light* and *dark green*

with the variable-resolution CESM model at 28 km (0.25°). The conclusions from this analysis are as follows.

First, the multi-model analysis of winter season SWE for the entire western USA mountain region showed that by 2040-2065 average SWE could decrease between −19% (NARCCAP) and −38% (VR-CESM). More resiliency in snowpack to climate change was seen in the interior mountain ranges (e.g., Rockies and Wasatch and Uinta) compared

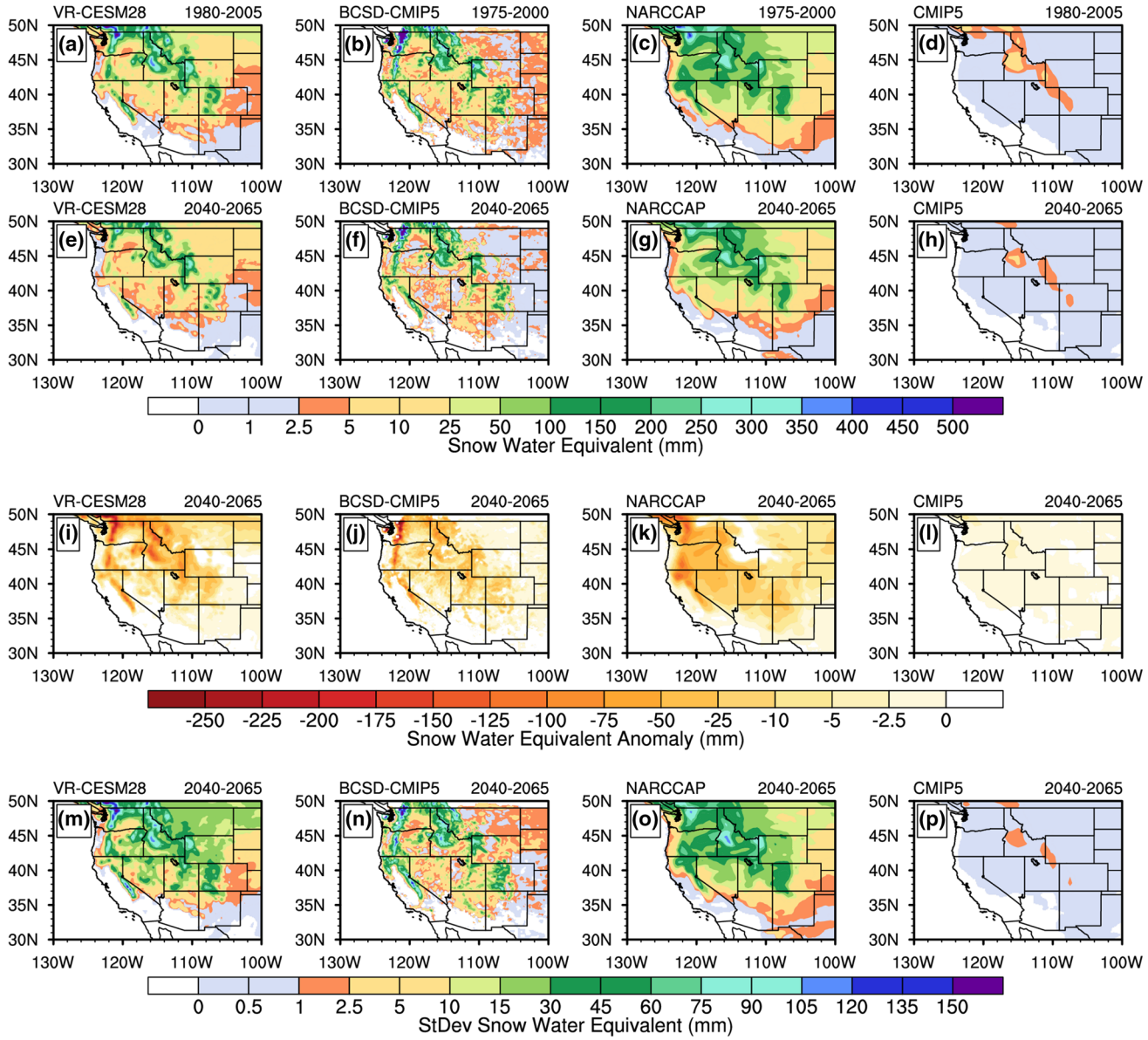

Fig. 5 The climate and seasonal (DJF) distributions and percent changes of SWE across the western USA within four global-to-regional climate change datasets. SWE climate average totals within pre-2005 (**a**–**e**) and RCP8.5 2040–2065 (**e**–**h**), SWE anomalies (**i**–**l**) and 2040–2065 seasonal (DJF) variability (**m**–**p**) are shown

to the coastal ranges (e.g., Cascades, Klamath, and Sierra Nevada) across all of the regionally downscaled datasets. This resiliency to the climate change signal is likely due to higher average elevation in the Rockies and Wasatch and Uinta mountain ranges, a larger distance to relatively warm ocean waters (which stabilizes surface temperatures), and less dependence on equatorial derived winter storm systems (particularly atmospheric rivers) compared to the coastal mountain ranges. Last, all of the regional downscaling models exhibited diminished interquartile ranges and maximum values, meaning that the snow distributions will diminish and snow deposition magnitudes will also decrease. This implies that seasonal snow deposition will become more predictable (as the variation collapses around the median), but total snow deposition will diminish overall. Regardless of the winter season variability differences, the collective median SWE value from all three datasets dropped by 27% throughout the western USA mountain ranges by 2065. The CMIP5 CESM global model ensemble, with no regional downscaling strategy, had negligible snowpack totals and was unusable for this analysis.

Second, the VR-CESM28 1980–2005 results were compared to several of the most high-quality and high-resolution spatially continuous datasets within the mountain

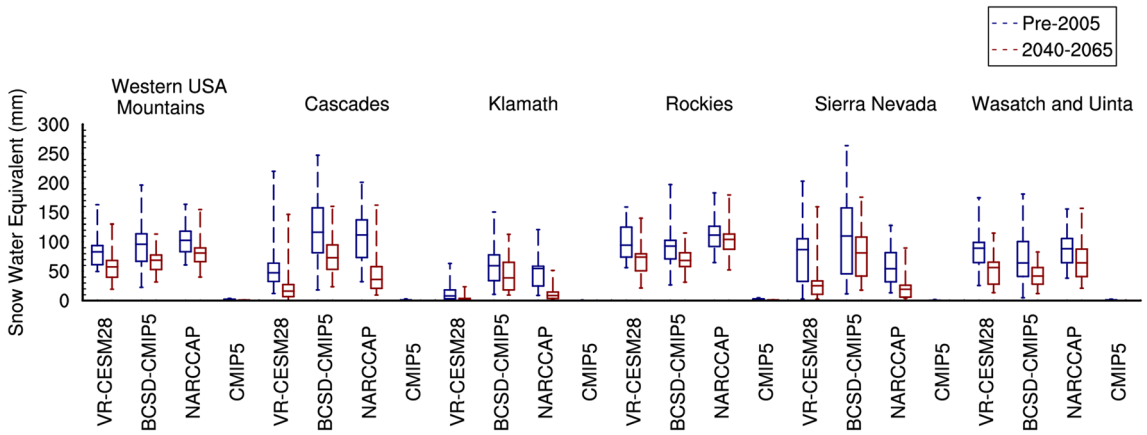

Fig. 6 The winter (DJF) season average box-and-whisker distributions of SWE across each of the western USA mountain ranges and each of the simulation periods. The *blue box*-and-whisker represents the 25 DJF seasons of pre-2005 simulations and the *red box*-and-whisker represents the 25 DJF simulated seasons from 2040 to 2065 forced by the business-as-usual (RCP8.5) scenario

research community. Compared to PRISM, peak accumulated precipitation within the total western USA mountain region was found to be positively biased in VR-CESM28 by +7% (818 mm for PRISM and 872 mm for VR-CESM28) and 2 mST is minimally biased in transitory seasons [i.e., Northern Hemisphere spring (MAM) and fall (SON)] and maximized in summer (JJA) and parts of the winter (DJF). By 2025–2050, the VR-CESM28 RCP8.5 climate change signal is within the range of bias for PRISM for PRECT and 2 mST, whereas by 2075–2100 the observed signal was outside this range. No quantitative conclusions were made about SWE bias in our simulations due to the lack of coherence in available datasets. The wide model spread is likely attributed to the use of land-surface models to abate spatial discontinuities in in-situ observations, the sparsity of in-situ observations in sampling the range of elevations and latitude/longitudes within a given mountain range, and, specifically to regional climate models, a lack of resolution of both topography and vegetative cover. In Rhoades et al. (2016), VR-CESM28 showed the tendency to have a early peak accumulation bias associated with too fast of a melt rate and too early total melt in a sub-region of the California Sierra Nevada when compared to SNOTEL in-situ observations. With that said, the VR-CESM28 SWE results fell in the middle of the available high-resolution SWE climate datasets analyzed, although deviations in the overall snowpack lifecycle (i.e., accumulation, peak timing and melt-rates) were observed. Therefore, the biased timing of peak snow accumulation and complete snow melt may partially explain the lack of agreement between simulated and observed hydroclimate variables. The simulated bias may be directly modulating 2 mST which in turn impacts the snow-albedo feedback.

Third, VR-CESM28 results were further analyzed over the 2025–2100 time period across several hydroclimate variables including snowfall, snow cover, SWE, 2 mST, and total precipitation. This was done to ensure a comprehensive assessment of the winter season western USA mountain hydrologic changes associated with RCP8.5 within a global-to-regional modeling framework. According to the Wilcoxon–Mann–Whitney rank-sum test, significant ($p < 0.05$) change from 1980 to 2005 PDFs for each of the hydroclimate variables varied by mountain range when assessing the 2025–2050 results, but were unanimous in the 2075–2100 results. Overall, VR-CESM28 projects a two-thirds reduction (−69%) in average mountain SWE with associated decrease in snow cover by nearly-half (−44%), an associated earlier peak snow accumulation and complete melt a month earlier (May), an uptick in mountainous total precipitation (+20%), with more rain and less snow (−24% drop in snow-to-rain ratio) and, lastly, and an amplified minimum (+5.8 °C), average (+5.0 °C), and maximum (+4.9 °C) mountain 2 mST. Notably, by the 2050s anomalously high winter season snowfall, snow cover, and SWE become almost non-existent with anomalously high 2 mST (+3 to +6 °C) becoming the new normal. The non-linear jump in 2 mST found in the VR-CESM28 projection simulations are likely indicative of a shift in the variability of the freezing line and a modification of the local snow cover. This variability is explained, in part, by the increase in magnitude of the interquartile ranges (i.e., the variability between colder and warmer seasons) and the diminished minimum anomalies (i.e., historically cold years). The increased variability of the freezing line and modification of snow cover creates a positive feedback loop by which the regional albedo is diminished and leads to more radiation being absorbed at the surface, positively amplifying the 2 mST.

Fourth, VR-CESM28 hydroclimate variables were further analyzed for elevational dependency within western

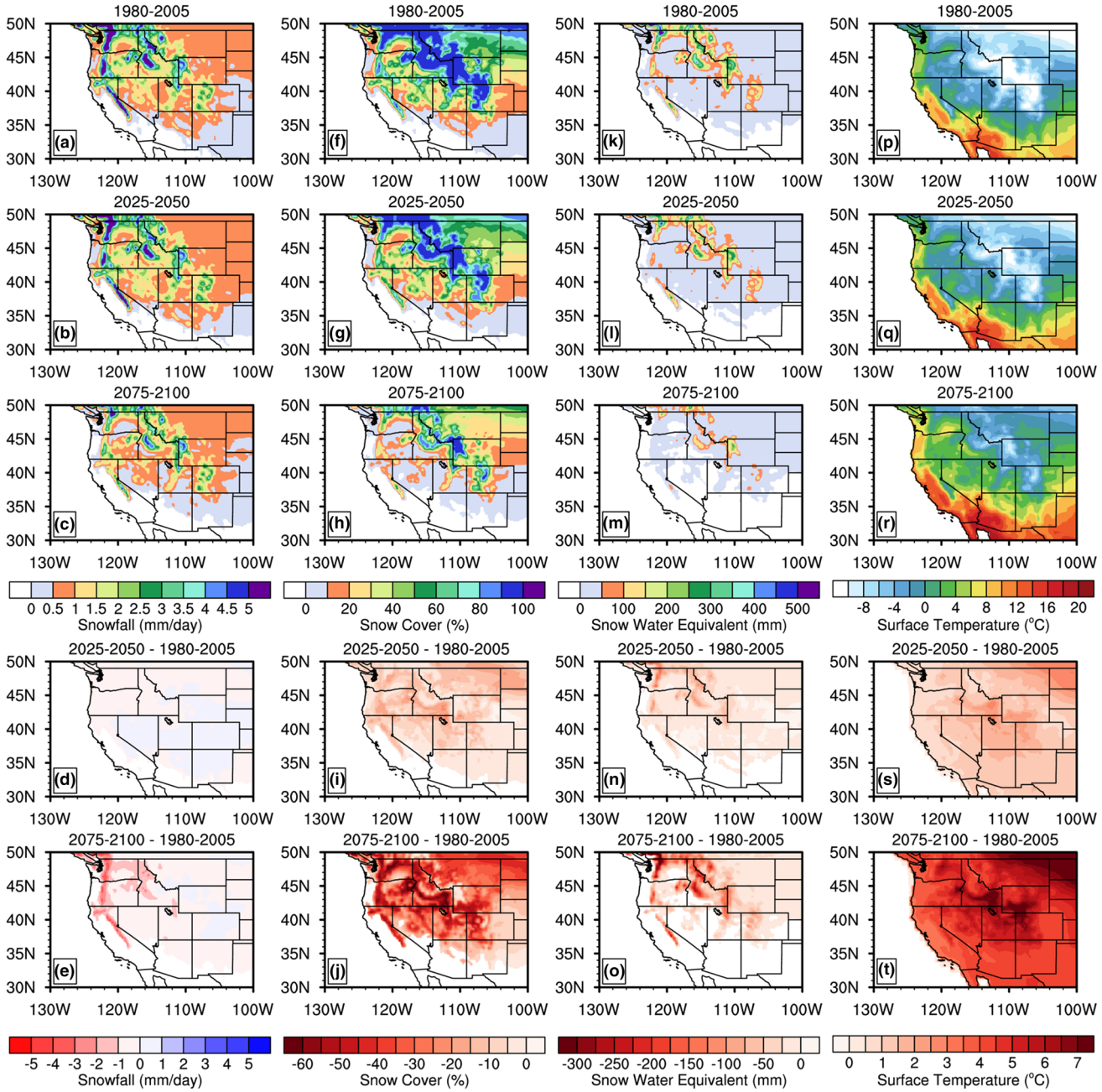

Fig. 7 A panel of VR-CESM28 winter (DJF) climatological averages of snowfall (**a**–**c**), snow cover (**f**–**h**), SWE (**k**–**m**), and 2-m surface temperature (**p**–**r**) for 1980–2005, 2025–2050, and 2075–2100 under the RCP8.5 scenario over the western USA. Climatological anomalies for the RCP8.5 scenario versus 1980–2005 are highlighted in the *bottom two rows*

USA mountain ranges. A notable nonlinear change in temperatures among the highest mountainous regions (i.e., the Rocky Mountains and the southern portion of the Sierra Nevada) was evident and supports the hypothesized phenomena known as elevation-dependent warming. For example, average (maximum) winter season 2 mST anomalies were +0.97 °C (+2.35 °C) from 500 to 1000 m and +2.85 °C (+7.01 °C) to +3.81 °C (+9.43 °C) from 1000 to >3000 m, with a maximized elevational warming between 2000 and 3000 m. In addition, the snowfall maxima did not always co-locate with the maxima snow cover elevation. This is likely a result of the variability of 2 mST around the freezing-line where peak snowfall is deposited in a region of high variability where at-or-below freezing 2 mST were not maintained and snow cover becomes more ephemeral. Snowfall at higher elevations (2000 to >2500 m) was nominally positive or negative; however, nonlinear negative change in snowfall was found as you progress

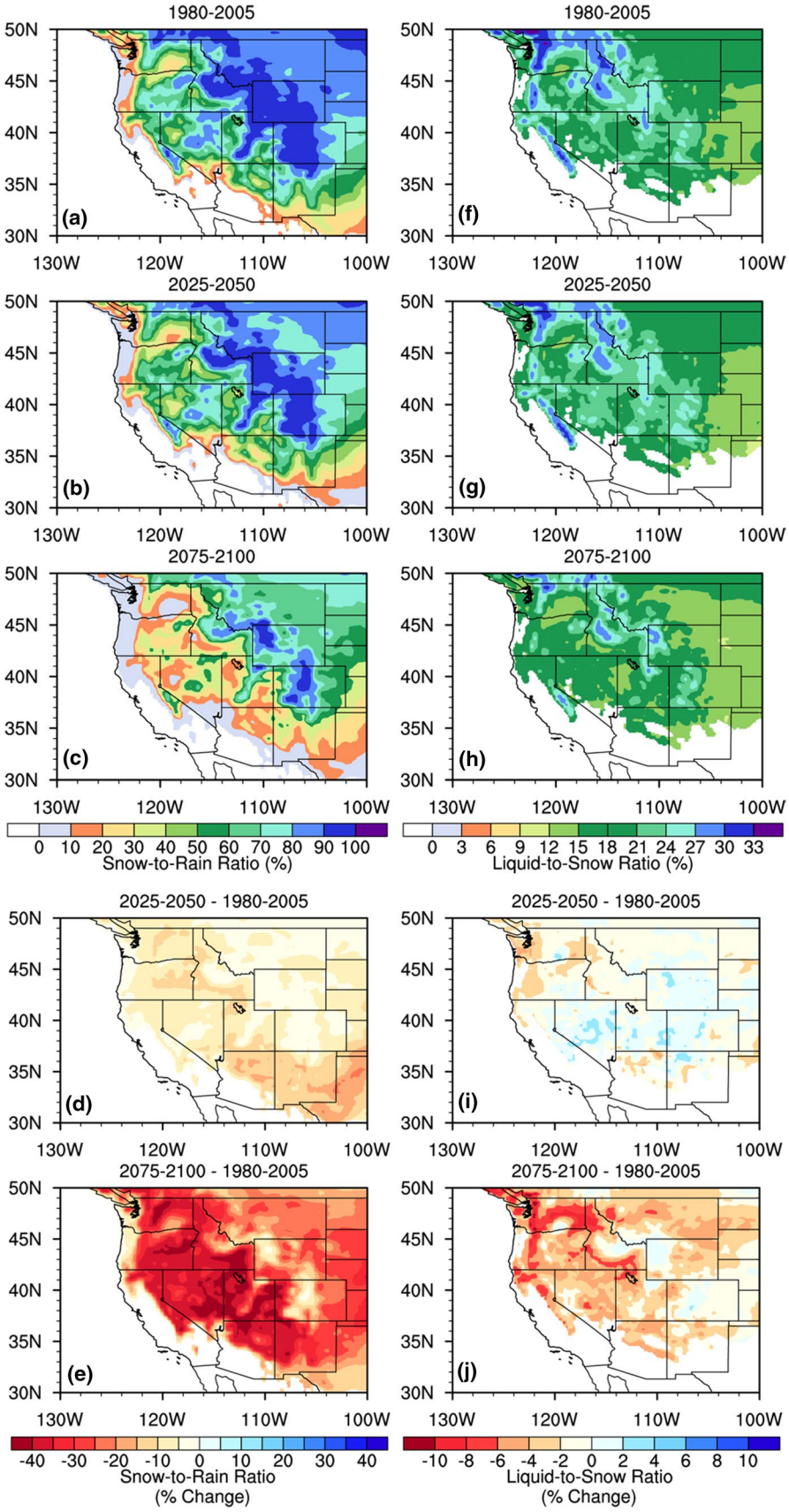

Fig. 8 Similar to Figure 7, however for snowfall-to-rainfall (**a**–**c**) and liquid-to-snow (**f**–**h**) ratios, with percent changes in each ratio highlighted under the DJF climatological averages (**d**, **e** and **i**, **j**)

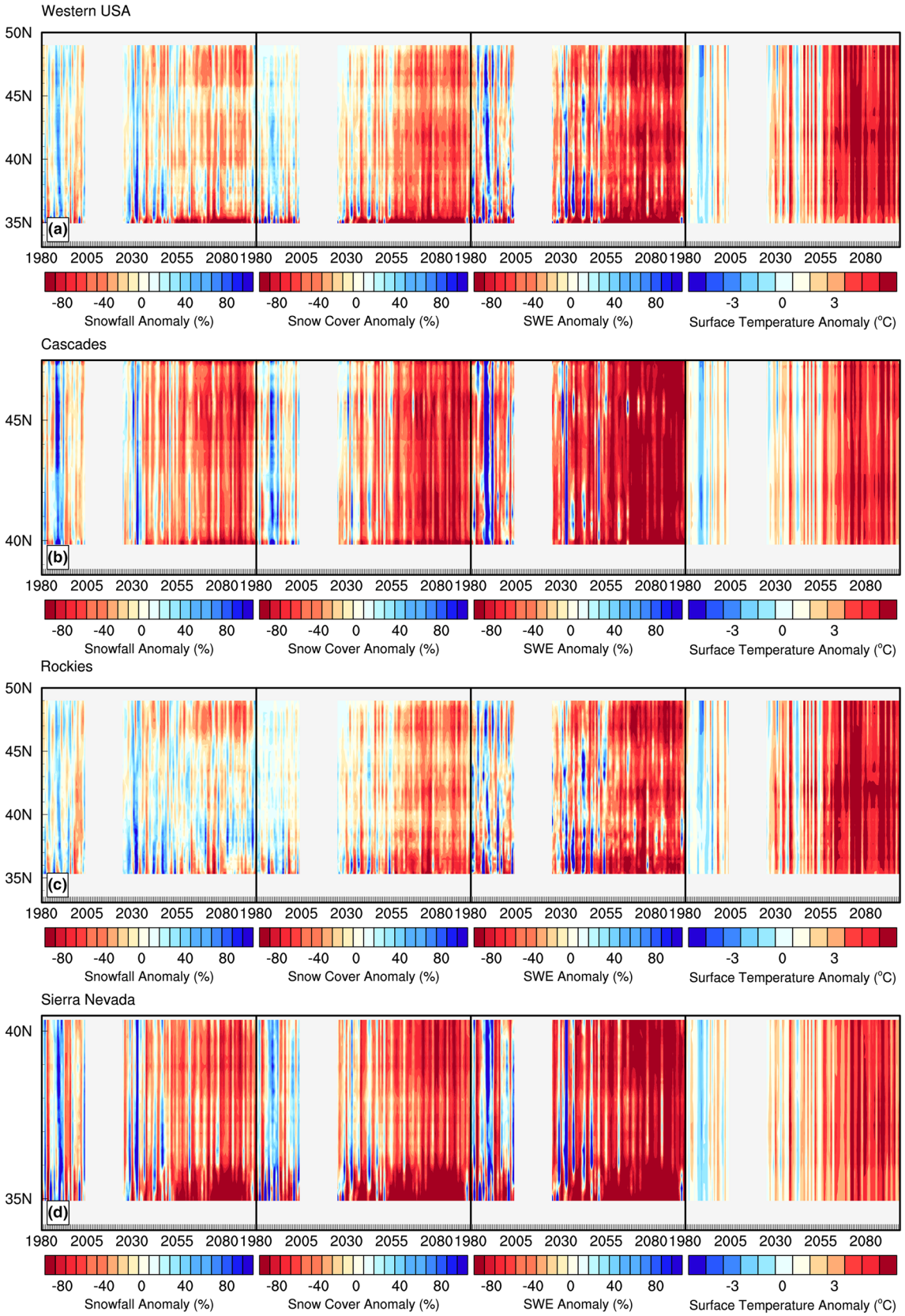

Fig. 9 Hovmöller diagram of the latitudinal average DJF total western USA mountain range (**a**), Cascades (**b**), Rockies (**c**), and Sierra Nevada (**d**), snowfall, snow cover, SWE, and 2 mST anomalies from the 1980–2005 DJF average. Regions of *red* (*blue*) indicate negative (positive) seasonal trends, save for 2-m surface temperature which has opposite color indication

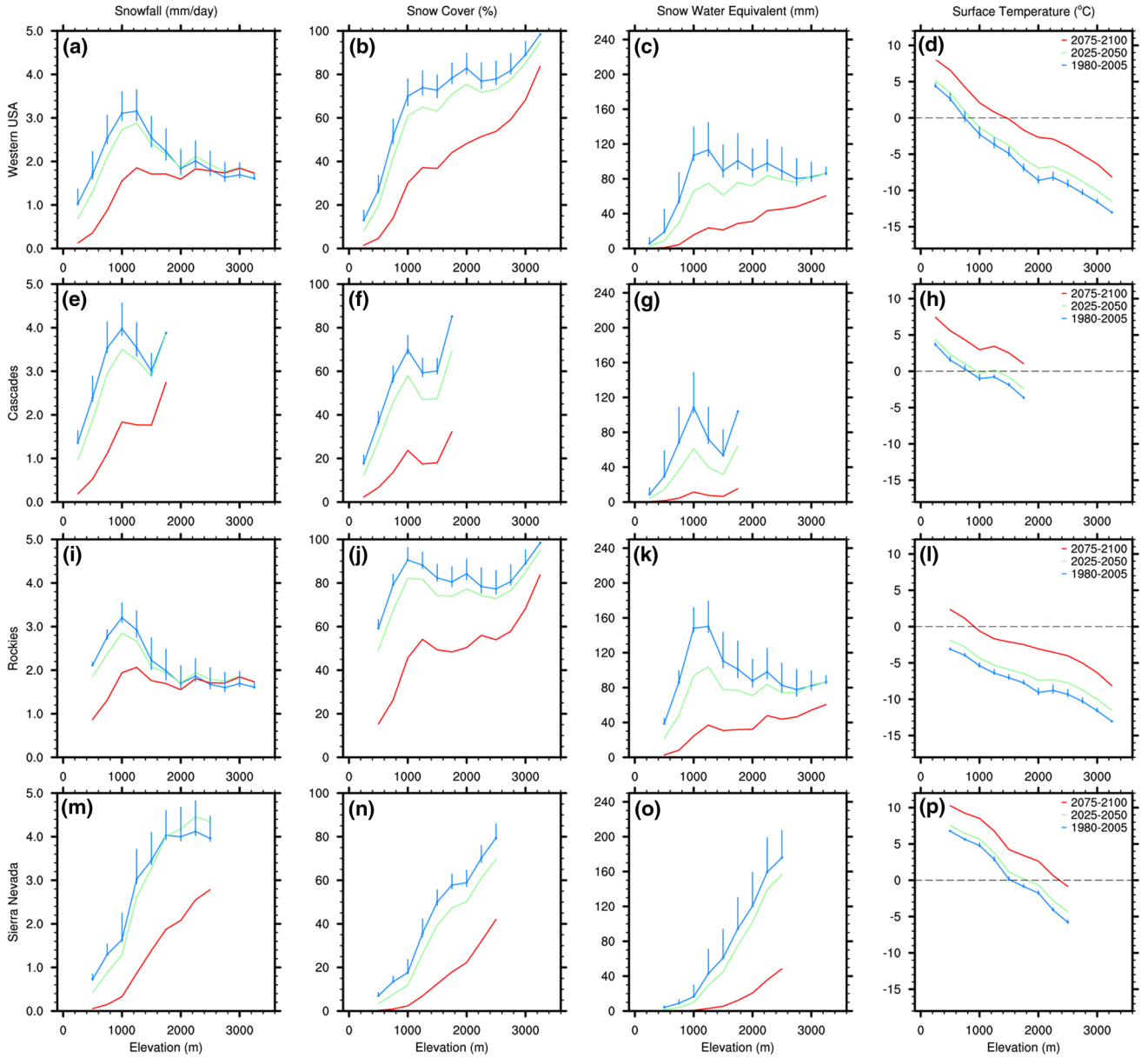

Fig. 10 Panel plot of western USA mountain range 250m DJF temporal and spatial average elevational profiles for snowfall, snow cover, SWE, and surface temperature for 1980–2005 (*blue*), 2025–2100 (*green*), and 2075–2100 (*red*) within VR-CESM28. The 250 m profiles for the total western USA mountain region are highlighted in **a**–**d**, Cascades in **e**–**h**, Rockies in **i**–**l**, and the Sierra Nevada **m**–**p**. To help in assessing historical simulated variability in comparison to the RCP8.5 forcing, sample *standard-error bars* were added at each elevation interval onto the historical simulation elevation profile. For surface temperature, a 0 °C temperature threshold (*freezing-line*) is plotted with a *dotted line* for visual guidance

downslope. Over 500 m intervals, snowfall dropped by −10.7% from 2000 to 1500 m, −16.6% from 1500 to 1000 m, and −20.9% from 1000 to 500 m. Interestingly, when compared to snowfall, both SWE and snow cover more linearly decreased downslope. Winter season average snow cover trends indicated a -5.7%/500 m to -6.8%/500 m, save for the change from 1000 to 500 m of −18.9%/500 m, and SWE trends showed a −11%/500 m to −15%/500 m. The average freezing line elevation in the western USA mountainous region shifted upwards from 750 m to 1500 m from 1980–2005 to 2075–2100. The 750 m upslope migration of the 1980–2005 freezing line was not uniform throughout each mountain range. Interior mountain ranges (e.g., Rockies and Wasatch and Uinta) maintain their freezing line at lower elevations compared to coastal ranges (e.g., Cascades, Klamath and Sierra Nevada). For example, the 1980–2005 average freezing line in the Cascades moved from 750 to 1750 m, the Rockies from 500 to 1000 m, and

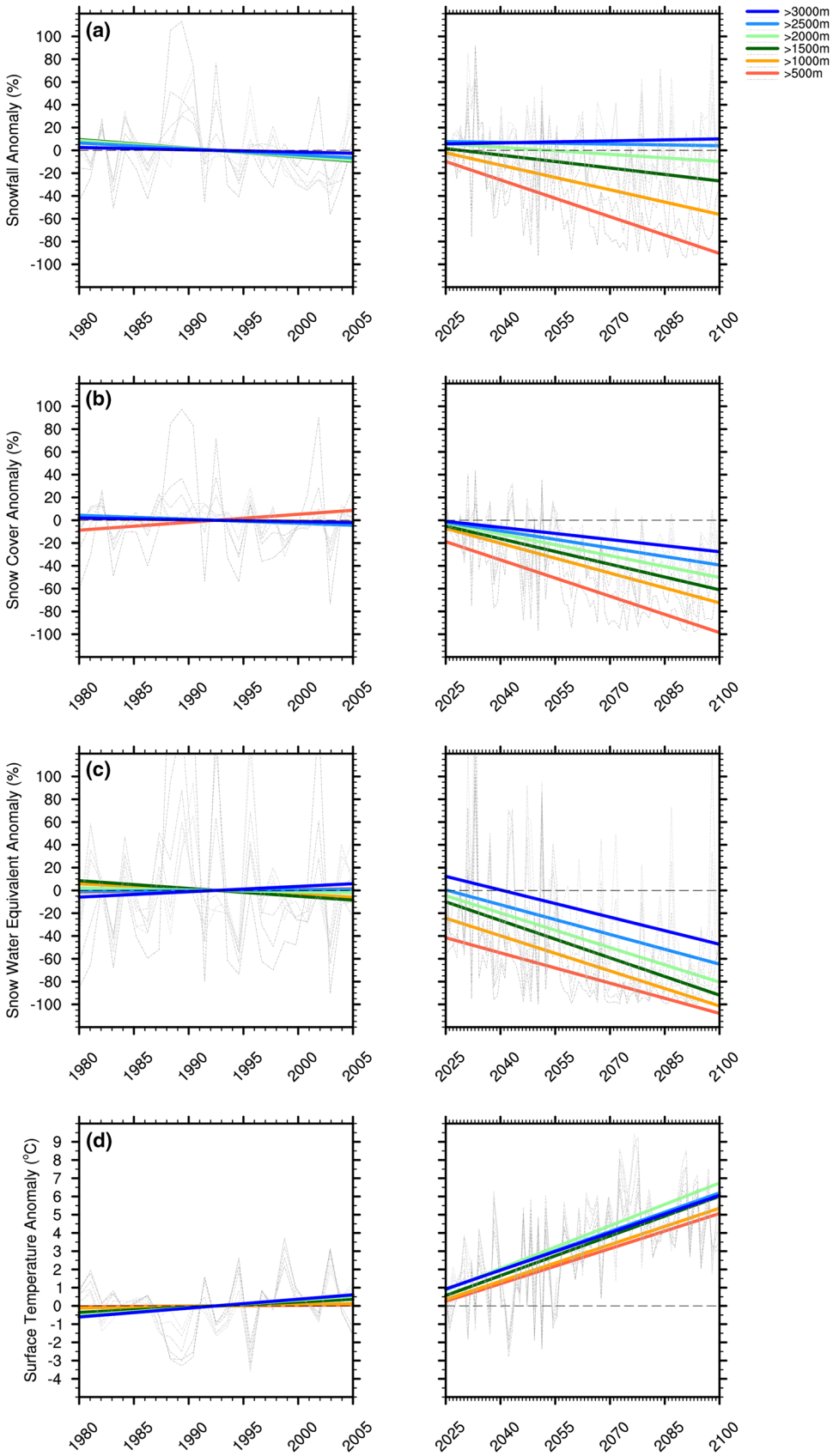

Fig. 11 Panel plot of 500 m interval elevation bands within the western USA mountain region for 1980–2005 and RCP8.5 2025–2100 DJF trends for **a** snowfall, **b** snow cover, **c** SWE, and **d** surface temperature anomalies for the VR-CESM28 simulations. The winter season variability for each 500 m elevation band are highlighted in a *lighter-to-darker grayscale dashed line* based on lower-to-higher elevation bands. A *dashed line* is drawn at the zero anomaly *y-intercept* for visual guidance

the Sierra Nevada from 1500 to 2250 m by 2075–2100. Overall, this implies that cities that fall within 750–1500 m (2450–4920 ft), such as those in the foothills of the western USA mountains (e.g., Reno, NV, Salt Lake City, UT, Idaho Falls, ID, and Yosemite Valley, CA), will experience less maintained snow accumulation than historically observed.

To continue the assessment of VR-CESM and its applicability to real world problems further research is needed. VR-CESM28 was only run at one resolution (28 km) with one topographic representation with the maximum elevation for these simulations at 3274 m across the western USA mountain region, or 1150 m below the highest peak in the western USA (Mt. Whitney). This singular topography choice was largely due to computational restraints as the focus was placed on running longer simulation time-frames. Therefore, the effects of orographic resolution and its associated forcing sensitivity will be assessed in future research. As shown in this study, VR-CESM28 may be too sensitive to orographic uplift as snowfall precipitates out too quickly at lower elevations and is not disbursed over larger bands of elevation, save for the Sierra Nevada. Thus, work is needed to understand how the variation in topographic resolution in VR-CESM impacts the hydroclimate trends in mountainous regions and the associated sensitivity to orographic uplift, rainfall transport and deposition. Coupled to this, a bias in the lifecycle of simulated SWE was found, but a complete analysis of the origin and development of this bias was out of the scope of this paper. As such, a targeted resolution increase in VR-CESM will be utilized over a selected mountain range to understand how CAM and CLM perform at a myriad of resolutions and where simulated bias begins to originate (or diminish).

Overall, VR-CESM28 results highlight a stronger climate change signal than other conventionally used datasets and, if the projections hold, will result in large ramifications for hydrologic managers of the western USA in the near-future. These changes will undoubtedly pressure western USA states to preemptively invest in climate adaptation measures such as alternative water storage, water-use efficiency, and reassess reservoir storage operations to ensure that a proper balance of allocations between the human-energy-environment nexus are maintained. Some of these climate adaptation strategies have already started in states such as California with the onset of its recent 2011-to-present unprecedented drought. With strong backing of policy and management, coupled with insights from the research community, California has taken pro-active steps to work towards better water management strategies. These strategies include more informed and targeted agricultural water allocations, mandatory reductions in urban water use, more stringent groundwater management and monitoring, and, finally, the reassessment of dated water right law from the 18th to 19th century Spanish settlement era which lead to large guaranteed appropriations of surface and groundwater to present day land owners and large cities (Hanak et al. 2011). More water management initiatives like this will be needed to ensure proper resiliency to unprecedented hydroclimate changes due to anthropogenic climate change.

Acknowledgements The authors would like to acknowledge Cecile Hannay for her help in ensuring that our RCP8.5 configuration within CESM was consistent with NCAR standards. We would also like to acknowledge the computational support, and patience, provided by the University of California, Davis Farm Cluster IT support team (i.e., Bill Broadley and Terri Knight). Further, we would like to thank our various research sponsors including: the National Science Foundation (NSF) via the Climate Change, Water, and Society Integrated Graduate Education and Research Traineeship (IGERT) program at the University of California, Davis (NSF Award Number: 1069333), the Leland Roy Saxon and Georgia Wood Saxon Fellowship, the "Multiscale Methods for Accurate, Efficient, and Scale-aware Models of the Earth System" within the Office of Science, Office of Biological and Environmental Research of the U.S. Department of Energy Earth System Modeling Program (ESM) under Contract No. DE-AC02-05CH11231. Support also comes from the California Agricultural Experiment Station (project CA-D-LAW-2203-H).

References

Anderson EA (1976) A point of energy and mass balance model of snow cover. NOAA Tech Rep NWS 19:1–150

Ashfaq M, Ghosh S, Kao SC, Bowling LC, Mote P, Touma D, Rauscher SA, Diffenbaugh NS (2013) Near-term acceleration of hydroclimatic change in the western US. J Geophys Res Atmos 118(19):10–676. doi:10.1002/jgrd.50816

Bacmeister JT, Wehner MF, Neale RB, Gettelman A, Hannay C, Lauritzen PH, Caron JM, Truesdale JE (2014) Exploratory high-resolution climate simulations using the community atmosphere model (CAM). J Clim 27(9):3073–3099. doi:10.1175/JCLI-D-13-00387.1

Bales RC, Molotch NP, Painter TH, Dettinger MD, Rice R, Dozier J (2006) Mountain hydrology of the western US. Water Resour Res 42(W08):432. doi:10.1029/2005WR004387

Bales RC, Rice R, Roy SB (2014) Estimated loss of snowpack storage in the Eastern Sierra Nevada with climate warming. J Water Resour Plan Manag 141(2):04014055. doi:10.1061/(ASCE)WR.1943-5452.0000453

Barnett TP, Pierce DW, Hidalgo HG, Bonfils C, Santer BD, Das T, Bala G, Wood AW, Nozawa T, Mirin AA et al (2008) Human-induced changes in the hydrology of the western US. Science 319(5866):1080–1083. doi:10.1126/science.1152538

Bartos MD, Chester MV (2015) Impacts of climate change on electric power supply in the Western US. Nat Clim Change. doi:10.1038/nclimate2648

Belmecheri S, Babst F, Wahl ER, Stahle DW, Trouet V (2016) Multi-century evaluation of Sierra Nevada snowpack. Nat Clim Change 6(1):2–3. doi:10.1038/nclimate2809

Berg N, Hall A, Sun F, Capps S, Walton D, Langenbrunner B, Neelin D (2015) Twenty-first-century precipitation changes over the Los Angeles region. J Clim 28(2):401–421. doi:10.1175/JCLI-D-14-00316.1

Berghuijs W, Woods R, Hrachowitz M (2014) A precipitation shift from snow towards rain leads to a decrease in streamflow. Nat Clim Change 4(7):583–586. doi:10.1038/nclimate2246

Brekke L, Thrasher B, Maurer E, Pruitt T (2013) Downscaled CMIP3 and CMIP5 climate and hydrology projections: release of downscaled CMIP5 climate projections, comparison with preceding information, and summary of user needs. US Dept of the Interior, Bureau of Reclamation, Technical Services Center, Denver

Cai X, Yang ZL, Xia Y, Huang M, Wei H, Leung LR, Ek MB (2014) Assessment of simulated water balance from Noah, Noah-MP, CLM, and VIC over CONUS using the NLDAS test bed. J Geophys Res Atmos 119(24):13–751. doi:10.1002/2014JD022113

Cannon AJ, Sobie SR, Murdock TQ (2015) Bias correction of GCM precipitation by quantile mapping: how well do methods preserve changes in quantiles and extremes? J Clim 28(17):6938–6959. doi:10.1175/JCLI-D-14-00754.1

Cayan DR (1996) Interannual climate variability and snowpack in the western US. J Clim 9:928–948. doi:10.1175/1520-0442(1996)009<0928:ICVASI>2.0.CO;2

Cayan DR, Redmond KT, Riddle LG (1999) ENSO and hydrologic extremes in the Western US. J Clim 12:2881–2893. doi:10.1175/1520-0442(1999) 012<2881:EAHEIT>2.0.CO;2

Chen F, Liu C, Dudhia J, Chen M (2014a) A sensitivity study of high-resolution regional climate simulations to three land surface models over the western United States. J Geophys Res Atmos 119(12):7271–7291. doi:10.1002/2014JD021827

Chen J, Brissette FP, Leconte R (2014b) Assessing regression-based statistical approaches for downscaling precipitation over North America. Hydrol Process 28(9):3482–3504. doi:10.1002/hyp.9889

Daly C, Halbleib M, Smith JI, Gibson WP, Doggett MK, Taylor GH, Curtis J, Pasteris PP (2008) Physiographically sensitive mapping of climatological temperature and precipitation across the conterminous United States. Int J Climatol 28(15):2031–2064. doi:10.1002/joc.1688

DeFlorio MJ, Pierce DW, Cayan DR, Miller AJ (2013) Western US extreme precipitation events and their relation to ENSO and PDO in CCSM4. J Clim 26(12):4231–4243. doi:10.1175/JCLI-D-12-00257.1

Dennis J, Edwards J, Evans KJ, Guba O, Lauritzen PH, Mirin AA, Str-Cyr A, Taylor MA, Worley PH (2011) CAM-SE: a scalable spectral element dynamical core for the community atmosphere model. Int J High Perfor Comput Appl:74–89. doi:10.1177/1094342011428142

Dettinger MD, Cayan DR (1995) Large-scale atmospheric forcing of recent trends toward early snowmelt runoff in California. J Clim 8:606–623. doi:10.1175/1520-0442(1995)008<0606:LSAFOR>2.0.CO;2

Diffenbaugh NS, Scherer M, Ashfaq M (2013) Response of snow-dependent hydrologic extremes to continued global warming. Nat Clim Change 3(4):379–384. doi:10.1038/nclimate1732

Field CB, Barros VR, Mastrandrea M, Mach KJ, Abdrabo MK, Adger N, Anokhin Y, Anisimov O, Arent D, Barnett J, et al. (2014) Summary for policymakers. Climate change 2014: impacts, adaptation, and vulnerability Part A: Global and Sectoral Aspects Contribution of Working Group II to the Fifth Assessment Report of the Intergovernmental Panel on Climate Change, pp 1–32. https://www.ipcc.ch/pdf/assessment-report/ar4/wg1/ar4-wg1-spm.pdf

Gates WL (1992) AMIP: the atmospheric model intercomparison project. Bull Am Meteorol Soc 73(12):1962–1970. doi:10.1175/1520-0477(1992)073<1962:ATAMIP>2.0.CO;2

Ghan SJ, Liu X, Easter RC, Zaveri R, Rasch PJ, Yoon JH, Eaton B (2012) Toward a minimal representation of aerosols in climate models: comparative decomposition of aerosol direct, semidirect, and indirect radiative forcing. J Clim 25(19):6461–6476. doi:10.1175/JCLI-D-11-00650.1

Glantz MH, Katz RW, Nicholls N (1991) Teleconnections linking worldwide climate anomalies. Cambridge University Press, Cambridge

Group MRIEW (2015) Elevation-dependent warming in mountain regions of the world. Nat Clim Change 5(5):424–430. doi:10.1038/nclimate2563

Groves DG, Yates D, Tebaldi C (2008) Developing and applying uncertain global climate change projections for regional water management planning. Water Resour Res 44(12): doi:10.1029/2008WR006964

Hall A (2004) The role of surface albedo feedback in climate. J Clim 17(7):1550–1568. doi:10.1175/1520-0442(2004)017<1550:TROSAF>2.0.CO;2

Hanak E, Lund J, Dinar A, Gray B, Howitt R, Mount J, Moyle P, Thompson B (2011) Managing Californias water from conflict to reconciliation. Public Policy Institute of California (PPIC). http://www.ppic.org/content/pubs/report/R_211EHR.pdf

Harris LM, Lin SJ (2013) A two-way nested global-regional dynamical core on the cubed-sphere grid. Mon Weather Rev 141(1):283–306. doi:10.1175/MWR-D-11-00201.1

Harris LM, Lin SJ, Tu C (2016) High-resolution climate simulations using GFDL HiRAM with a stretched global grid. J Clim 29(11):4293–4314. doi:10.1175/JCLI-D-15-0389.1

Henn B, Clark M, Kavetski D, Newman A, Hughes M, McGurk B, Lundquist J (2016) Spatiotemporal patterns of precipitation inferred from streamflow observations across the Sierra Nevada mountain range. J Hydrol. doi:10.1016/j.jhydrol.2016.08.009

Huang X, Ullrich PA (2016) Irrigation impacts on California's climate with the variable-resolution CESM. J Adv Model Earth Syst. doi:10.1002/2016MS000656

Huang X, Rhoades AM, Ullrich PA, Zarzycki CM (2016) An evaluation of the variable-resolution CESM for modeling California's climate. J Adv Model Earth Syst 8:345–369. doi:10.1002/2015MS000559

Hurrell JW, Hack JJ, Shea D, Caron JM, Rosinski J (2008) A new sea surface temperature and sea ice boundary dataset for the community atmosphere model. J Clim 21(19):5145–5153. doi:10.1175/2008JCLI2292.1

Iacono MJ, Delamere JS, Mlawer EJ, Shephard MW, Clough SA, Collins WD (2008) Radiative forcing by long-lived greenhouse gases: calculations with the AER radiative transfer models. J Geophys Res Atmos 113(D13). doi:10.1029/2008JD009944

Kinter JL, Cash B, Achuthavarier D, Adams J, Altshuler E, Dirmeyer P, Doty B, Huang B, Jin EK, Marx L, Manganello J, Stan C, Wakefield T, Palmer T, Hamrud M, Jung T, Miller M, Towers P, Wedi N, Satoh M, Tomita H, Kodama C, Nasuno T, Oouchi K, Yamada Y, Taniguchi H, Andrews P, Baer T, Ezell M, Halloy C, John D, Loftis B, Mohr R, Wong K (2013) Revolutionizing climate modeling with project athena: a multi-institutional international collaboration. Bull Am Meteorol Soc 94(2):231–245. doi:10.1175/BAMS-D-11-00043.1

Jordan R (1991) A one-dimensional temperature model for a snow cover: technical documentation for SNTHERM. 89. Tech. Rep., DTIC Document

Kapnick S, Hall A (2012) Causes of recent changes in western North American snowpack. Clim Dyn 38:1885–1899. doi:10.1007/s00382-011-1089-y

Kay JE, Deser C, Phillips A, Mai A, Hannay C, Strand G, Arblaster JM, Bates SC, Danabasoglu G, Edwards J, Holland M, Kushner P, Lamarque JF, Lawrence D, Lindsay K, Middleton A, Munoz E, Neale R, Oleson K, Polvani L, Vertenstein M (2015) The community earth system model (CESM) large ensemble project: a community resource for studying climate change in the presence of internal climate variability. Bull Am Meteorol Soc 96(8):1333–1349. doi:10.1175/BAMS-D-13-00255.1

Klos PZ, Link TE, Abatzoglou JT (2014) Extent of the rain-snow transition zone in the western US under historic and projected climate. Geophys Res Lett 41(13):4560–4568. doi:10.1002/2014GL060500, L060500

Lawrence DM, Oleson KW, Flanner MG, Thornton PE, Swenson SC, Lawrence PJ, Zeng X, Yang ZL, Levis S, Sakaguchi K, Bonan GB, Slater AG (2011) Parameterization improvements and functional and structural advances in version 4 of the Community Land Model. J Adv Model Earth Syst 3. doi:10.1029/2011MS000045

Li W, Forest CE (2014) Estimating the sensitivity of the atmospheric teleconnection patterns to SST anomalies using a linear statistical method. J Clim 27(24):9065–9081. doi:10.1175/JCLI-D-14-00231.1

Lute AC, Abatzoglou JT, Hegewisch KC (2015) Projected changes in snowfall extremes and interannual variability of snowfall in the western United States. Water Resourc Res 51(2):960–972. doi:10.1002/2014WR016267

Margulis SA, Corts G, Girotto M, Durand M (2016a) A Landsat-Era Sierra Nevada snow reanalysis (1985–2015). J Hydrometeorol 17(4):1203–1221. doi:10.1175/JHM-D-15-0177.1

Margulis SA, Corts G, Girotto M, Huning LS, Li D, Durand M (2016b) Characterizing the extreme 2015 snowpack deficit in the Sierra Nevada (USA) and the implications for drought recovery. Geophys Res Lett:6341–6349. doi:10.1002/2016GL068520, 2016GL068520

Maurer E, Hidalgo H, Das T, Dettinger M, Cayan D (2010) Assessing climate change impacts on daily streamflow in California: the utility of daily large-scale climate data. Hydrol Earth Syst Sci Discuss 7(1):1209–1243. doi:10.5194/hess-14-1125-2010

Maurer EP, Brekke L, Pruitt T, Duffy PB (2007) Fine-resolution climate projections enhance regional climate change impact studies. Eos Trans Am Geophys Union 88(47):504–504. doi:10.1029/2007EO470006

McCorquodale P, Ullrich PA, Johansen H, Colella P (2015) An adaptive multiblock high-order finite-volume method for solving the shallow-water equations on the sphere. Commun Appl Math Comput Sci 10:121–162. doi:10.2140/camcos.2015.10.121

Mearns LO, Gutowski WJ, Jones R, Leung LY, McGinnis S, Nunes AMB, Qian Y (2009) A regional climate change assessment program for North America. EoS 90(36):311–312. doi:10.1175/BAMS-D-11-00223.1

Mearns LO, Arritt R, Biner S, Bukovsky MS, McGinnis S, Sain S, Caya D Jr, JC, Flory D, Gutowski W, Takle ES, Jones R, Leung R, Moufouma-Okia W, McDaniel L, Nunes AMB, Qian Y, Roads J, Sloan L, Snyder M, (2012) The North American Regional Climate Change Assessment Program: overview of phase I results. Bull Am Meteorol Soc 93(9):1337–1362. doi:10.1175/BAMS-D-11-00223.1

Mearns LO, Sain S, Leung LR, Bukovsky MS, McGinnis S, Biner S, Caya D, Arritt RW, Gutowski W, Takle E, Snyder M, Jones RG, Nunes AMB, Tucker S, Herzmann D, McDaniel L, Sloan L (2013) Climate change projections of the North American Regional Climate Change Assessment Program (NARCCAP). Clim Change 120(4):965–975. doi:10.1007/s10584-013-0831-3

Morrison H, Gettelman A (2008) A new two-moment bulk stratiform cloud microphysics scheme in the community atmosphere model, version 3 (CAM3). Part I: description and numerical tests. J Clim 21(15):3642–3659. doi:10.1175/2008JCLI2105.1

Mote PW, Hamlet AF, Clark MP, Lettenmaier DP (2005) Declining mountain snowpack in western North America. Bull Am Meteorol Soc 86:39–49. doi:10.1175/BAMS-86-1-39

National Climate Assessment (accessed 2016) Southwest. http://nca2014.globalchange.gov/report/regions/southwest

National Geophysical Data Center (2006) 2-minute Gridded Global Relief Data (ETOPO2) v2. National Geophysical Data Center, NOAA. 2014: doi:10.7289/V5J1012Q

Neale RB, Richter JH, Jochum M (2008) The impact of convection on ENSO: from a delayed oscillator to a series of events. J Clim 21(22):5904–5924. doi:10.1175/2008JCLI2244.1

Neale RB, Chen CC, Gettelman A, Lauritzen PH, Park S, Williamson DL, Conley AJ, Garcia R, Kinnison D, Lamarque JF, Marsh D, Mills M, Smith AK, Tilmes S, Vitt F, Cameron-Smith P, Collins WD, Iacono MJ, , Easter RC, Liu X, Ghan SJ, Rasch PJ, Taylor MA (2010) Description of the NCAR community atmosphere model (CAM 5.0). NCAR Technical Note NCAR/TN-486+STR, National Center for Atmospheric Research, Boulder, Colorado

Oleson K, Lawrence D, Bonan G, Flanner M, Kluzek E, Lawrence P, Levis S, Swenson S, Thornton P, Dai A, Decker M, Dickinson R, Feddema J, Heald C, Hoffman F, Lamarque J, Mahowald N, Niu G, Qian T, Randerson J, Running S, Sakaguchi K, Slater A, Stockli R, Wang A, Yang Z, Zeng X, Zeng X (2010) Technical Description of version 4.0 of the Community Land Model (CLM). NCAR Technical Note NCAR/TN-478+STR, National Center for Atmospheric Research, Boulder, Colorado. doi:10.5065/D6FB50WZ

Painter TH, Berisford DF, Boardman JW, Bormann KJ, Deems JS, Gehrke F, Hedrick A, Joyce M, Laidlaw R, Marks D, Mattmann C, McGurk B, Ramirez P, Richardson M, Skiles SM, Seidel FC, Winstral A (2016) The airborne snow observatory: fusion of scanning lidar, imaging spectrometer, and physically-based modeling for mapping snow water equivalent and snow albedo. Remote Sens Environ 184:139–152. doi:10.1016/j.rse.2016.06.018

Palmer PL (1988) The SCS snow survey water supply forecasting program: current operations and future directions. In: Proceedings western snow conference, pp 43–51. http://westernsnowconference.org/sites/westernsnowconference.org/PDFs/1988Palmer.pdf

Pandey GR, Cayan DR, Georgakakos KP (1999) Precipitation structure in the Sierra Nevada of California during winter. J Geophys Res Atmos 104(D10):12019–12030. doi:10.1029/1999JD900103

Park S, Bretherton CS (2009) The University of Washington shallow convection and moist turbulence schemes and their impact on climate simulations with the community atmosphere model. J Clim 22(12):3449–3469. doi:10.1175/2008JCLI2557.1

Park S, Bretherton CS, Rasch PJ (2014) Integrating cloud processes in the community atmosphere model, Version 5. J Clim 27(18):6821–6856. doi:10.1175/JCLI-D-14-00087.1

Pavelsky TM, Kapnick S, Hall A (2011) Accumulation and melt dynamics of snowpack from a multiresolution regional climate model in the central Sierra Nevada, California. J Geophys Res Atmos:116. doi:10.1029/2010JD015479

Pavelsky TM, Sobolowski S, Kapnick SB, Barnes JB (2012) Changes in orographic precipitation patterns caused by a shift from snow to rain. Geophys Res Lett:39. doi:10.1029/2012GL052741

Pierce DW, Cayan DR (2013) The uneven response of different snow measures to human-induced climate warming. J Clim 26:4148–4167. doi:10.1175/JCLI-D-12-00534.1

Pierce DW, Das T, Cayan DR, Maurer EP, Miller NL, Bao Y, Kanamitsu M, Yoshimura K, Snyder MA, Sloan LC et al (2013) Probabilistic estimates of future changes in California temperature and precipitation using statistical and dynamical downscaling. Clim Dyn 40(3–4):839–856. doi:10.1007/s00382-012-1337-9

Pierce DW, Cayan DR, Maurer EP, Abatzoglou JT, Hegewisch KC (2015) Improved bias correction techniques for hydrological

simulations of climate change. J Hydrometeorol 16(6):2421–2442. doi:10.1175/JHM-D-14-0236.1

Qu X, Hall A (2014) On the persistent spread in snow-albedo feedback. Clim Dyn 42(1–2):69–81. doi:10.1007/s00382-013-1774-0

Rauscher SA, Ringler TD (2014) Impact of variable-resolution meshes on midlatitude baroclinic eddies using CAM-MPAS-A. Mon Weather Rev 142(11):4256–4268. doi:10.1175/MWR-D-13-00366.1

Rauscher SA, Ringler TD, Skamarock WC, Mirin AA (2013) Exploring a global multiresolution modeling approach using aquaplanet simulations. J Clim 26(8):2432–2452. doi:10.1175/JCLI-D-12-00154.1

Rhoades AM, Huang X, Ullrich PA, Zarzycki CM (2016) Characterizing sierra nevada snowpack using variable-resolution CESM. J Appl Meteorol Climatol 55(1):173–196. doi:10.1175/JAMC-D-15-0156.1

Rupp DE, Mote PW, Bindoff NL, Stott PA, Robinson DA (2013) Detection and attribution of observed changes in Northern Hemisphere spring snow cover. J Clim 26:6904–6914. doi:10.1175/JCLI-D-12-00563.1

Salzmann N, Mearns LO (2012) Assessing the performance of multiple regional climate model simulations for seasonal mountain snow in the upper Colorado River basin. J Hydrometeorol 13(2):539–556. doi:10.1175/2011JHM1371.1

Schulzweida U, Kornblueh L, Quast R (2007) CDO User's guide–climate data operators. Tech. rep., Max Planck Institute, version 1.0.7, Tech. Rep. http://www.mpimet.mpg.de/fileadmin/software/cdo

Skamarock WC, Klemp JB, Duda MG, Fowler LD, Park SH, Ringler TD (2012) A multiscale nonhydrostatic atmospheric model using centroidal Voronoi tesselations and C-grid staggering. Mon Weather Rev 140:3090–3105. doi:10.1175/MWR-D-11-00215.1

Small RJ, Bacmeister J, Bailey D, Baker A, Bishop S, Bryan F, Caron J, Dennis J, Gent P, Hm Hsu, Jochum M, Lawrence D, Muoz E, diNezio P, Scheitlin T, Tomas R, Tribbia J, Tseng Yh, Vertenstein M (2014a) A new synoptic scale resolving global climate simulation using the community earth system model. J Adv Model Earth Syst 6(4):1065–1094. doi:10.1002/2014MS000363

Small RJ, Bacmeister J, Bailey D, Baker A, Bishop S, Bryan F, Caron J, Dennis J, Gent P, Hm Hsu et al (2014b) A new synoptic scale resolving global climate simulation using the community earth system model. J Adv Model Earth Syst 6(4):1065–1094. doi:10.1002/2014MS000363

Stewart IT (2009) Changes in snowpack and snowmelt runoff for key mountain regions. Hydrol Process 23:78–94. doi:10.1002/hyp.7128

Taylor KE, Stouffer RJ, Meehl GA (2012) An overview of CMIP5 and the experiment design. Bull Am Meteorol Soc 93(4):485–498. doi:10.1175/BAMS-D-11-00094.1

Taylor M, Tribbia J, Iskandarani M (1997) The spectral element method for the shallow water equations on the sphere. J Comput Phys 130:92–108. doi:10.1006/jcph.1996.5554

Taylor MA, Fournier A (2010) A compatible and conservative spectral element method on unstructured grids. J Comput Phys 229(17):5879–5895. doi:10.1016/j.jcp.2010.04.008

Toure AM, Rodell M, Yang ZL, Beaudoing H, Kim E, Zhang Y, Kwon Y (2016) Evaluation of the Snow Simulations from the community land model, version 4 (CLM4). J Hydrometeorol 17(1):153–170. doi:10.1175/JHM-D-14-0165.1

Ullrich (2014) SQuadGen: spherical quadrilateral grid generator. http://climate.ucdavis.edu/squadgen.php

Ullrich PA, Taylor MA (2015) Arbitrary-order conservative and consistent remapping and a theory of linear maps: part I. Mon Weather Rev 143(6):2419–2440. doi:10.1175/MWR-D-14-00343.1

Ullrich PA, Devendran D, Johansen H (2016) Arbitrary-order conservative and consistent remapping and a theory of linear maps, part 2. Mon Weather Rev 144(4):1529–1549. doi:10.1175/MWR-D-15-0301.1

Velázquez JA, Troin M, Caya D, Brissette F (2015) Evaluating the time-invariance hypothesis of climate model bias correction: implications for hydrological impact studies. J Hydrometeorol 16(5):2013–2026. doi:10.1175/JHM-D-14-0159.1

Wallace JM, Gutzler DS (1981) Teleconnections in the geopotential height field during the Northern Hemisphere winter. Monthly Weather Review 109(4):784–812. doi:10.1175/1520-0493(1981) 109<0784:TITGHF>2.0.CO;2

Wang SY, Hipps L, Gillies RR, Yoon JH (2014) Probable causes of the abnormal ridge accompanying the 2013–2014 California drought: ENSO precursor and anthropogenic warming footprint. Geophys Res Lett 41(9):3220–3226. doi:10.1002/2014GL059748

Wehner MF, Bala G, Duffy P, Mirin AA, Romano R (2010) Towards direct simulation of future tropical cyclone statistics in a high-resolution global atmospheric model. Adv Meteorol 2010:13. doi:10.1155/2010/915303

van der Wiel K, Kapnick SB, Vecchi GA, Cooke WF, Delworth TL, Jia L, Murakami H, Underwood S, Zeng F (2016) The resolution dependence of contiguous US precipitation extremes in response to CO_2 forcing. J Clim 29(22):7991–8012. doi:10.1175/JCLI-D-16-0307.1

Wise EK (2012) Hydroclimatology of the US intermountain west. Progr Phys Geogr 36:458–479. doi:10.1177/0309133312446538

Xia Y, Mitchell K, Ek M, Cosgrove B, Sheffield J, Luo L, Alonge C, Wei H, Meng J, Livneh B, et al. (2012a) Continental-scale water and energy flux analysis and validation for North American Land Data Assimilation System project phase 2 (NLDAS-2): 2. Validation of model-simulated streamflow. J Geophys Res Atmos 117(D3). doi:10.1029/2011JD016051

Xia Y, Mitchell K, Ek M, Sheffield J, Cosgrove B, Wood E, Luo L, Alonge C, Wei H, Meng J, et al. (2012b) Continental-scale water and energy flux analysis and validation for the North American Land Data Assimilation System project phase 2 (NLDAS-2): 1. Intercomparison and application of model products. J Geophys Res Atmos 117(D3). doi:10.1029/2011JD016048

Yongjiu D, Qingcun Z (1997) A land surface model (IAP94) for climate studies part I: formulation and validation in off-line experiments. Adv Atmos Sci 14:433–460. doi:10.1007/s00376-997-0063-4

Zarzycki CM, Jablonowski C (2014) A multidecadal simulation of Atlantic tropical cyclones using a variable-resolution global atmospheric general circulation model. J Adv Model Earth Syst 6(3):805–828. doi:10.1002/2014MS000352

Zarzycki CM, Jablonowski C, Taylor MA (2014a) Using variable resolution meshes to model tropical cyclones in the community atmosphere model. Mon Weather Rev 142(3):1221–1239. doi:10.1175/MWR-D-13-00179.1

Zarzycki CM, Levy MN, Jablonowski C, Overfelt JR, Taylor MA, Ullrich PA (2014b) Aquaplanet experiments using CAM's variable-resolution dynamical core. J Clim 27:5481–5503. doi:10.1175/JCLI-D-14-00004.1

Zarzycki CM, Jablonowski C, Thatcher DR, Taylor MA (2015) Effects of localized grid refinement on the general circulation and climatology in the community atmosphere model. J Clim 28(7):2777–2803. doi:10.1175/JCLI-D-14-00599.1

Zender CS (2008) Analysis of self-describing gridded geoscience data with netCDF operators (NCO). Environ Model Softw 23(10):1338–1342. doi:10.1016/j.envsoft.2008.03.004